

Supplementary Information

**Molecular imaging of plant-microbe interactions on the
Brachypodium seed surface**

Yuchen Zhang,^a Rachel Komorek,^a Jiyoung Son,^a Shawn Riechers,^a Zihua Zhu,^b Janet Jansson,^c
Christer Jansson,^b and Xiao-Ying Yu^{*a}

^a Energy and Environment Directorate, Pacific Northwest National Laboratory, Richland, WA 99354, USA

^b Environmental Molecular Science Laboratory, Pacific Northwest National Laboratory, Richland, WA 99354, USA

^c Earth and Biological Science Directorate, Pacific Northwest National Laboratory, Richland, WA 99354, USA

* Corresponding Author, e-mail: xiaoying.yu@pnnl.gov

Keywords: PGPR • *Brachypodium distachyon* • ToF-SIMS • metabolite • host • delayed extraction

Table of Contents

Supplemental Figures.....	S-1
Fig. S1. <i>Pseudomonas fluorescens</i> (<i>P.</i>) and <i>Arthrobacter chlorophenolicus</i> sp. nov. (<i>A.</i>) biofilm culture setup using the SALVI device.....	S-1
Fig. S2a. ToF-SIMS spectral reproducibility of the DI control seed of the top section in the negative mode ($m/z^- 0 - 200$).....	S-2
Fig. S2b. ToF-SIMS spectral reproducibility of the DI control seed of the top section in the negative mode ($m/z^- 200 - 400$).....	S-3
Fig. S3a. ToF-SIMS spectral reproducibility of the DI control seed in the bottom section in the negative mode ($m/z^- 0 - 200$).....	S-4
Fig. S3b. ToF-SIMS spectral reproducibility of the DI control seed of the bottom section in the negative mode ($m/z^- 200 - 400$).....	S-5
Fig. S4a. ToF-SIMS spectral reproducibility of the DI control seed of the top section in the positive mode ($m/z^+ 0 - 200$).....	S-6
Fig. S4b. ToF-SIMS spectral reproducibility of the DI control seed of the top section in the positive mode ($m/z^+ 200 - 400$).....	S-7
Fig. S5a. ToF-SIMS spectral reproducibility of the DI control seed of the bottom section in the positive mode ($m/z^+ 0 - 200$).....	S-8
Fig. S5b. ToF-SIMS spectral reproducibility of the DI control seed of the bottom section in the positive mode ($m/z^+ 200 - 400$).....	S-9
Fig. S6a. ToF-SIMS spectral comparison among three treatments of the top seed sections in the negative mode ($m/z^- 0 - 400$).....	S-10
Fig. S6b. ToF-SIMS spectral comparison among three treatments of the bottom seed sections in the negative mode ($m/z^- 0 - 400$).....	S-11
Fig. S7a. ToF-SIMS spectral comparison among three treatments of the top seed sections in the positive mode ($m/z^+ 0 - 400$).....	S-12
Fig. S7b. ToF-SIMS spectral comparison among three treatments of the bottom seed sections in the positive mode ($m/z^+ 0 - 400$).....	S-13
Fig. S8a. ToF-SIMS spectral comparison of the top section of the dry seed, DI control seed, <i>P.</i> -treated seed, and the <i>P.</i> -bacteria control in the negative mode ($m/z^- 0 - 400$).....	S-14
Fig. S8b. ToF-SIMS spectral comparison of the bottom section of the dry seed, DI control seed, <i>P.</i> -treated seed, and the <i>P.</i> -bacteria control in the negative mode ($m/z^- 0 - 400$).....	S-15
Fig. S9a. ToF-SIMS spectral comparison of the top section of the dry seed, DI control seed, <i>P.</i> -treated seed, and the <i>P.</i> -bacteria control in the positive mode ($m/z^+ 0 - 400$).....	S-16
Fig. S9b. ToF-SIMS spectral comparison of the bottom section of the dry seed, DI control seed, <i>P.</i> -treated seed, and the <i>P.</i> -bacteria control in the positive mode ($m/z^+ 0 - 400$).....	S-17

Supplementary Information

- Fig. S10a.** ToF-SIMS spectral comparison of the top section of the dry seed, DI control seed, *A.*-treated seed, and the *A.*-bacteria control in the negative mode ($m/z^- 0 - 400$).S-18
- Fig. S10b.** ToF-SIMS spectral comparison of the bottom section of the dry seed, DI control seed, *A.*-treated seed, and the *A.*-bacteria control in the negative mode ($m/z^- 0 - 400$).S-19
- Fig. S11a.** ToF-SIMS spectral comparison in the top section of the dry seed, DI control seed, *A.*-treated seed, and the *A.*-bacteria control in the positive mode ($m/z^+ 0 - 400$).S-20
- Fig. S11b.** ToF-SIMS spectral comparison in the bottom section of the dry seed, DI control seed, *A.*-treated seed, and *A.*-bacteria control seed in the positive mode ($m/z^+ 0 - 400$).S-21
- Fig. S12.** All peak spectral PCA results: (a) PC1 and PC2 scores plot, (b) PC1 loadings plot, and (c) PC2 loadings plot of *P.*-treated samples in the positive mode ($m/z^+ 0 - 800$).S-22
- Fig. S13.** All peak spectral PCA results: (a) PC1 and PC2 scores plot, (b) PC1 loadings plot, and (c) PC2 loadings plot of *A.*-treated samples in the positive mode ($m/z^+ 0 - 800$).S-23
- Fig. S14.** Selected peak spectral PCA results: (a) PC2 and PC4 scores plot, (b) PC2 loadings plot, and (c) PC4 loadings plot of *P.*-treated samples in the negative mode ($m/z^- 100 - 400$).
..... S-24
- Fig. S15.** Selected peak spectral PCA results: (a) PC3 and PC4 scores plot, (b) PC3 loadings plot, and (c) PC4 loadings plot of *A.*-treated samples in the negative mode ($m/z^- 100 - 400$).
.....S-25
- Fig. S16.** Selected peak spectral PCA results: (a) PC1 and PC2 scores plot, (b) PC1 loadings plot, and (c) PC2 loadings plot of *P.*-treated samples in the positive mode ($m/z^+ 100 - 400$).
.....S-26
- Fig. S17.** Selected peak spectral PCA results: (a) the PC1 and PC2 scores plot, (b) PC1 loadings plot, and (c) PC2 loadings plot of *A.*-treated samples in the positive mode ($m/z^+ 100 - 400$).S-27
- Fig. S18.** The normalized comparison bar plots between the DI control seed and *P.*-treated seed in the negative ion mode ($m/z^- 100 - 400$).S-28
- Fig. S19.** The normalized comparison bar plots between the DI control seed and *A.*-treated seed in the negative ion mode ($m/z^- 100 - 400$).S-29
- Fig. S20.** Delayed extraction 2D the DI control seed of the top section in the negative mode: (a) total ions, (b) fragment of quercetin $[^{1,2}\text{B}]^-$ ($m/z^- 120.99$, $\text{C}_7\text{H}_5\text{O}_2^-$), (c) p-hydroxybenzoic acid ($m/z^- 137.02$, $\text{C}_7\text{H}_5\text{O}_3^-$), (d) cinnamic acid ($m/z^- 147.04$, $\text{C}_9\text{H}_7\text{O}_2^-$), (e) palmitic acid ($m/z^- 255.13$, $\text{C}_{16}\text{H}_{31}\text{O}_2^-$), and (f) stearic acid ($m/z^- 283.29$, $\text{C}_{18}\text{H}_{35}\text{O}_2^-$). The scanning areas are $500 \times 500 \mu\text{m}^2$S-30
- Fig. S21.** Delayed extraction 2D images of the *P.*-treated seed of the top section in the negative mode: (a) total ions, (b) fragment of quercetin $[^{1,2}\text{B}]^-$ ($m/z^- 120.99$, $\text{C}_7\text{H}_5\text{O}_2^-$), (c) p-hydroxybenzoic acid ($m/z^- 137.02$, $\text{C}_7\text{H}_5\text{O}_3^-$), (d) cinnamic acid ($m/z^- 147.04$, $\text{C}_9\text{H}_7\text{O}_2^-$), (e) palmitic acid ($m/z^- 255.13$, $\text{C}_{16}\text{H}_{31}\text{O}_2^-$), and (f) stearic acid ($m/z^- 283.29$, $\text{C}_{18}\text{H}_{35}\text{O}_2^-$). The scanning areas are $500 \times 500 \mu\text{m}^2$S-31

Supplementary Information

Fig. S22. Delayed extraction 2D images of the <i>A.</i> -treated seed of the top section in the negative mode: (a) total ions, (b) fragment of quercetin ^[1, 2B] ⁻ (m/z^- 120.99, C ₇ H ₅ O ₂ ⁻), (c) p-hydroxybenzoic acid (m/z^- 137.02, C ₇ H ₅ O ₃ ⁻), (d) cinnamic acid (m/z^- 147.04, C ₉ H ₇ O ₂ ⁻), (e) palmitic acid (m/z^- 255.13, C ₁₆ H ₃₁ O ₂ ⁻), and (f) stearic acid (m/z^- 283.29, C ₁₈ H ₃₅ O ₂ ⁻). The scanning areas are 500 × 500 μm ² .	S-32
Fig. S23. Delayed extraction 2D images of the DI control seed of the bottom section in the negative mode: (a) total ions, (b) fragment of quercetin ^[1, 2B] ⁻ (m/z^- 120.99, C ₇ H ₅ O ₂ ⁻), (c) p-hydroxybenzoic acid (m/z^- 137.02, C ₇ H ₅ O ₃ ⁻), (d) cinnamic acid (m/z^- 147.04, C ₉ H ₇ O ₂ ⁻), (e) palmitic acid (m/z^- 255.13, C ₁₆ H ₃₁ O ₂ ⁻), and (f) stearic acid (m/z^- 283.29, C ₁₈ H ₃₅ O ₂ ⁻). The scanning areas are 500 × 500 μm ² .	S-33
Fig. S24. Delayed extraction 2D images of the <i>P.</i> -treated seed of the bottom section in the negative mode: (a) total ions, (b) fragment of quercetin ^[1, 2B] ⁻ (m/z^- 120.99, C ₇ H ₅ O ₂ ⁻), (c) p-hydroxybenzoic acid (m/z^- 137.02, C ₇ H ₅ O ₃ ⁻), (d) cinnamic acid (m/z^- 147.04, C ₉ H ₇ O ₂ ⁻), (e) palmitic acid (m/z^- 255.13, C ₁₆ H ₃₁ O ₂ ⁻) and (f) stearic acid (m/z^- 283.29, C ₁₈ H ₃₅ O ₂ ⁻). The scanning areas are 500 × 500 μm ² .	S-34
Fig. S25. Delayed extraction 2D images of the <i>A.</i> -treated seed of the bottom section in the negative mode: (a) total ions, (b) fragment of quercetin ^[1, 2B] ⁻ (m/z^- 120.99, C ₇ H ₅ O ₂ ⁻), (c) p-hydroxybenzoic acid (m/z^- 137.02, C ₇ H ₅ O ₃ ⁻), (d) cinnamic acid (m/z^- 147.04, C ₉ H ₇ O ₂ ⁻), (e) palmitic acid (m/z^- 255.13, C ₁₆ H ₃₁ O ₂ ⁻), and (f) stearic acid (m/z^- 283.29, C ₁₈ H ₃₅ O ₂ ⁻). The scanning areas are 500 × 500 μm ² .	S-35
Fig. S26. High resolution 2D images of the <i>Seteria</i> leaf in the negative mode: (a) total ions, (b) fragment of quercetin ^[1, 2B] ⁻ (m/z^- 120.99, C ₇ H ₅ O ₂ ⁻), (c) p-hydroxybenzoic acid (m/z^- 137.02, C ₇ H ₅ O ₃ ⁻), (d) cinnamic acid (m/z^- 147.04, C ₉ H ₇ O ₂ ⁻), (e) palmitic acid (m/z^- 255.13, C ₁₆ H ₃₁ O ₂ ⁻), and (f) stearic acid (m/z^- 283.29, C ₁₈ H ₃₅ O ₂ ⁻). The scanning areas are 200 × 200 μm ² .	S-36
Fig. S27. Delayed extraction 2D images of the <i>Seteria</i> leaf in the negative mode: (a) total ions, (b) fragment of quercetin ^[1, 2B] ⁻ (m/z^- 120.99, C ₇ H ₅ O ₂ ⁻), (c) p-hydroxybenzoic acid (m/z^- 137.02, C ₇ H ₅ O ₃ ⁻), (d) cinnamic acid (m/z^- 147.04, C ₉ H ₇ O ₂ ⁻), (e) palmitic acid (m/z^- 255.13, C ₁₆ H ₃₁ O ₂ ⁻), and (f) stearic acid (m/z^- 283.29, C ₁₈ H ₃₅ O ₂ ⁻). The scanning areas are 200 × 200 μm ² .	S-37
Fig. S28. Delayed extraction 2D total ion images of (a) DI control, (b) <i>P.</i> -treated, and (c) <i>A.</i> -treated <i>Brachypodium</i> seed top sections and their corresponding spectra (d-f) in m/z^+ 100 – 400 in the positive mode.	S-38
Fig. S29. Delayed extraction 2D total ion images of (a) DI control, (b) <i>P.</i> -treated, and (c) <i>A.</i> -treated <i>Brachypodium</i> seed bottom sections and their corresponding spectra (d-f) in m/z^+ 100 – 400 in the positive mode.	S-39
Supplemental Tables	S-40
Table S1. The mass resolution of selected peaks of the delayed extraction mode.	S-40
Table S2. Possible peak identification in the negative ion mode.	S-41
Table S3. Possible peak identification in the positive ion mode.	S-42

Supplementary Information

Table S4. Representative fatty acid reference spectral information in the negative and positive ion mode.....	S-43
References.....	S-44

Supplementary Information

Supplemental information was provided to substantiate the discussion and provide additional experimental details including figures, tables, and associated references.

Supplemental Figures

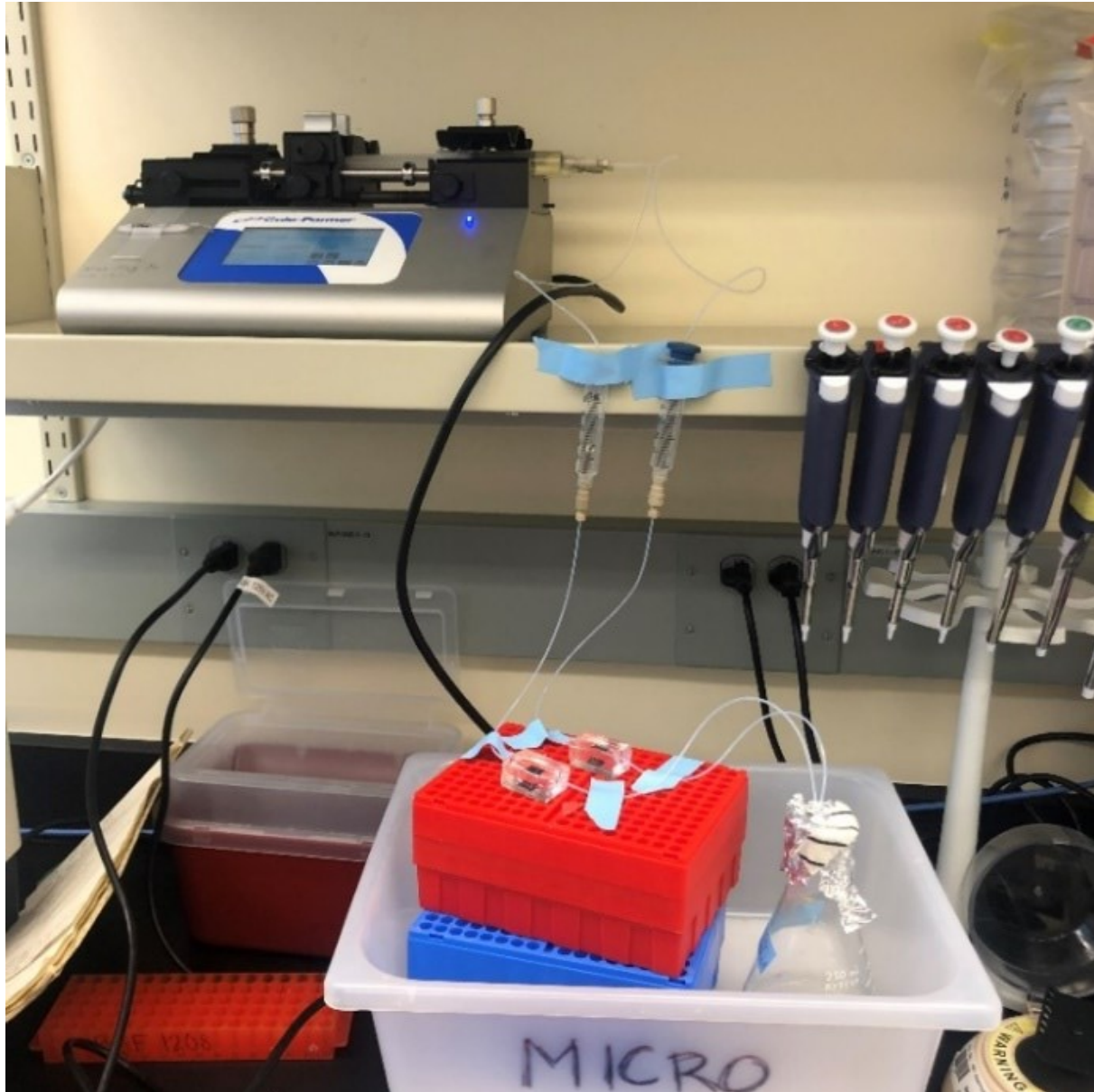


Fig. S1. *Pseudomonas fluorescens* (*P.*) and *Arthrobacter chlorophenolicus* sp. nov. (*A.*) biofilm culture setup using the SALVI device.

This picture shows the bubble trap and overall setup for biofilm culture in the SALVI microreactor. Visible *P.* and *A.* biofilms were observed in the microchannel after culture started for five to six days.

Supplementary Information

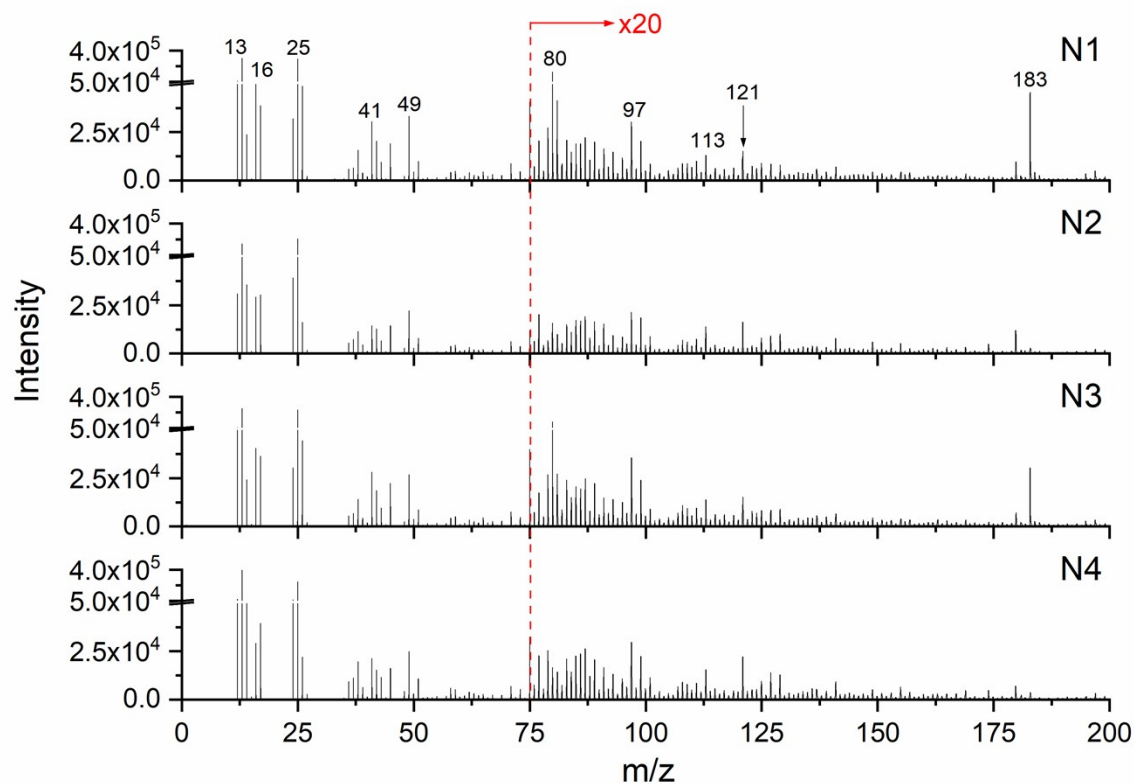


Fig. S2a. ToF-SIMS spectral reproducibility of the DI control seed of the top section in the negative mode (m/z^- 0 – 200).

N1, N2, N3, and N4 represent the first, second, third, and fourth negative ion mode data acquired consecutively in the DI control seed section.

Supplementary Information

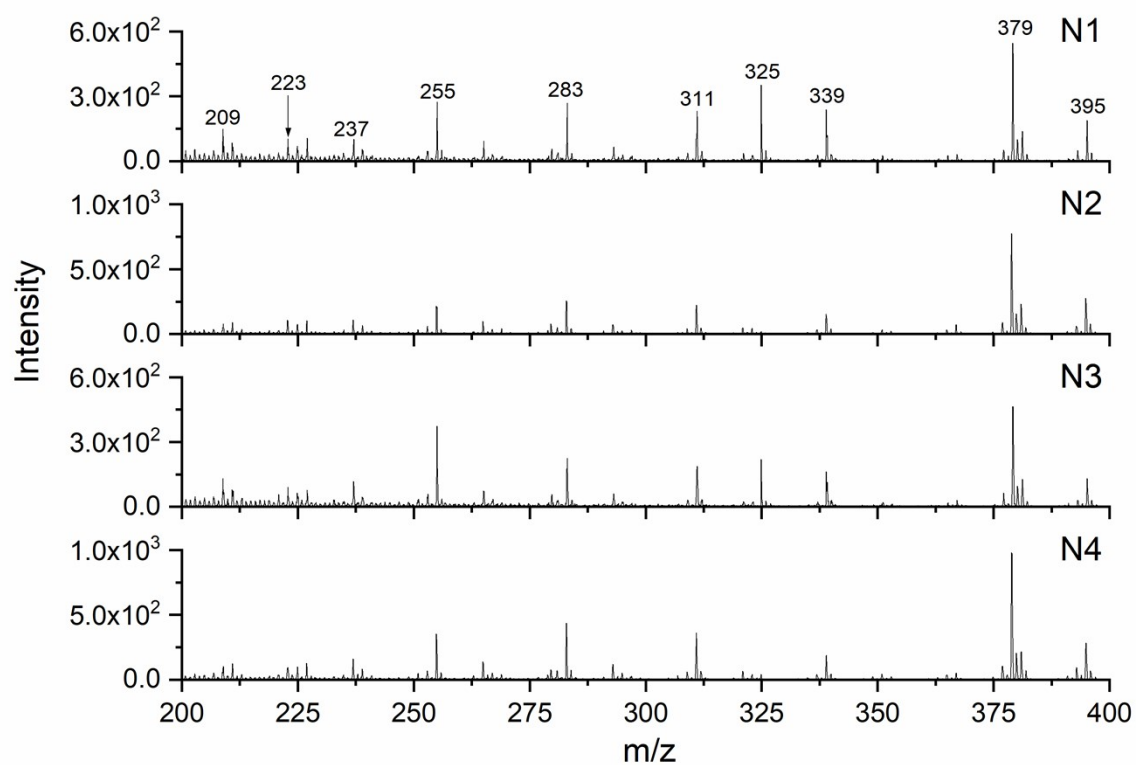


Fig. S2b. ToF-SIMS spectral reproducibility of the DI control seed of the top section in the negative mode (m/z^- 200 – 400).

N1, N2, N3, and N4 represent the first, second, third, and fourth negative ion mode data acquired consecutively in the DI control seed section.

Supplementary Information

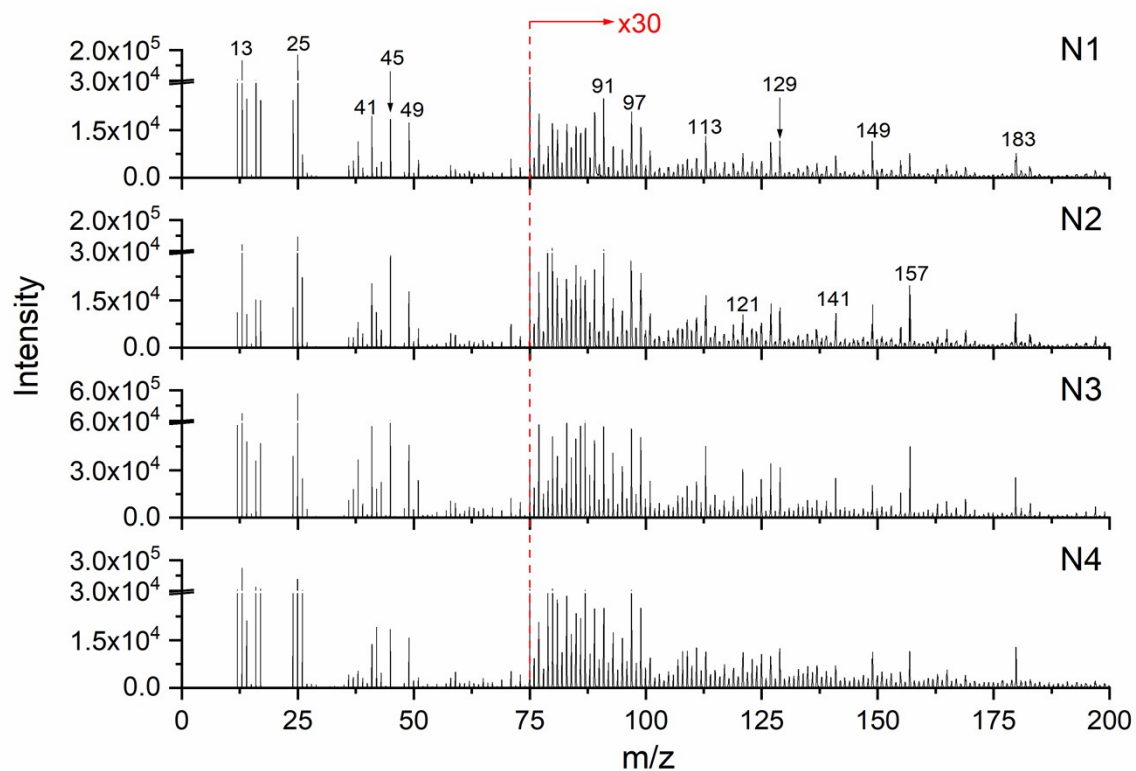


Fig. S3a. ToF-SIMS spectral reproducibility of the DI control seed in the bottom section in the negative mode (m/z^- 0 – 200).

N1, N2, N3, and N4 represent the first, second, third, and fourth negative ion mode data acquired consecutively in the DI control seed section.

Supplementary Information

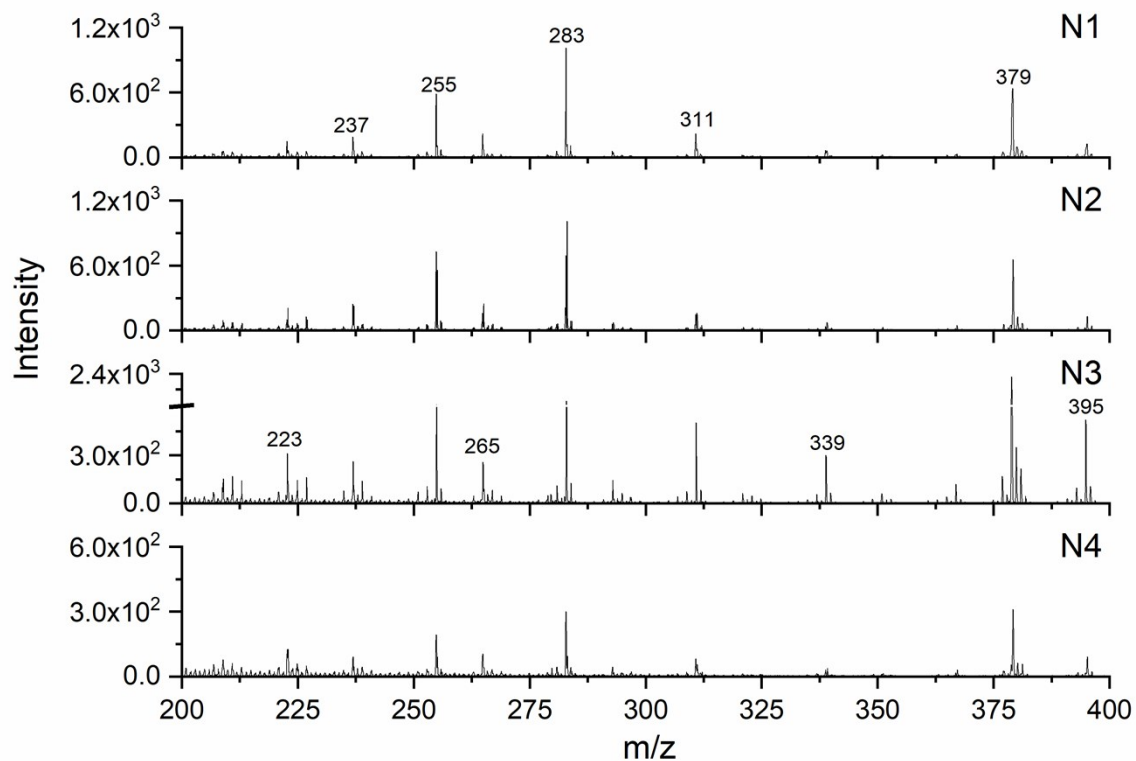


Fig. S3b. ToF-SIMS spectral reproducibility of the DI control seed of the bottom section in the negative mode (m/z^- 200 – 400).

N1, N2, N3, and N4 represent the first, second, third, and fourth negative ion mode data acquired consecutively in the DI control seed section.

Supplementary Information

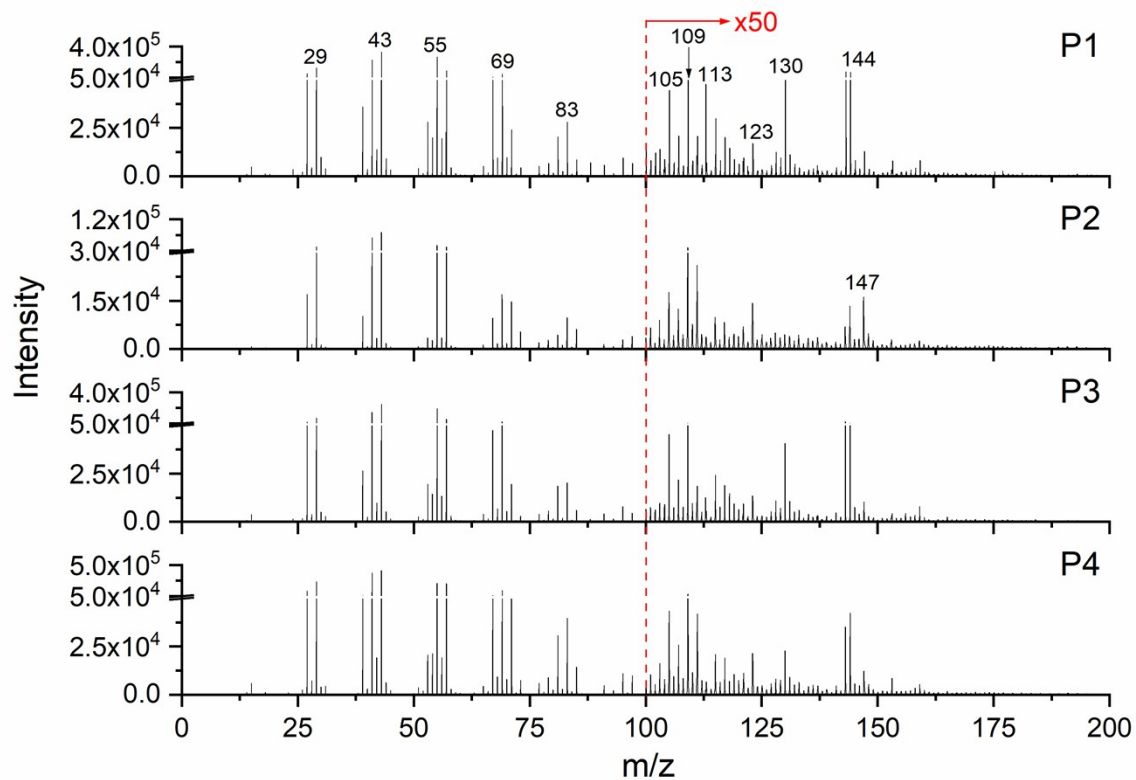


Fig. S4a. ToF-SIMS spectral reproducibility of the DI control seed of the top section in the positive mode ($m/z^+ 0 - 200$).

P1, P2, P3, and P4 represent the first, second, third, and fourth positive ion mode data acquired consecutively in the DI control seed section.

Supplementary Information

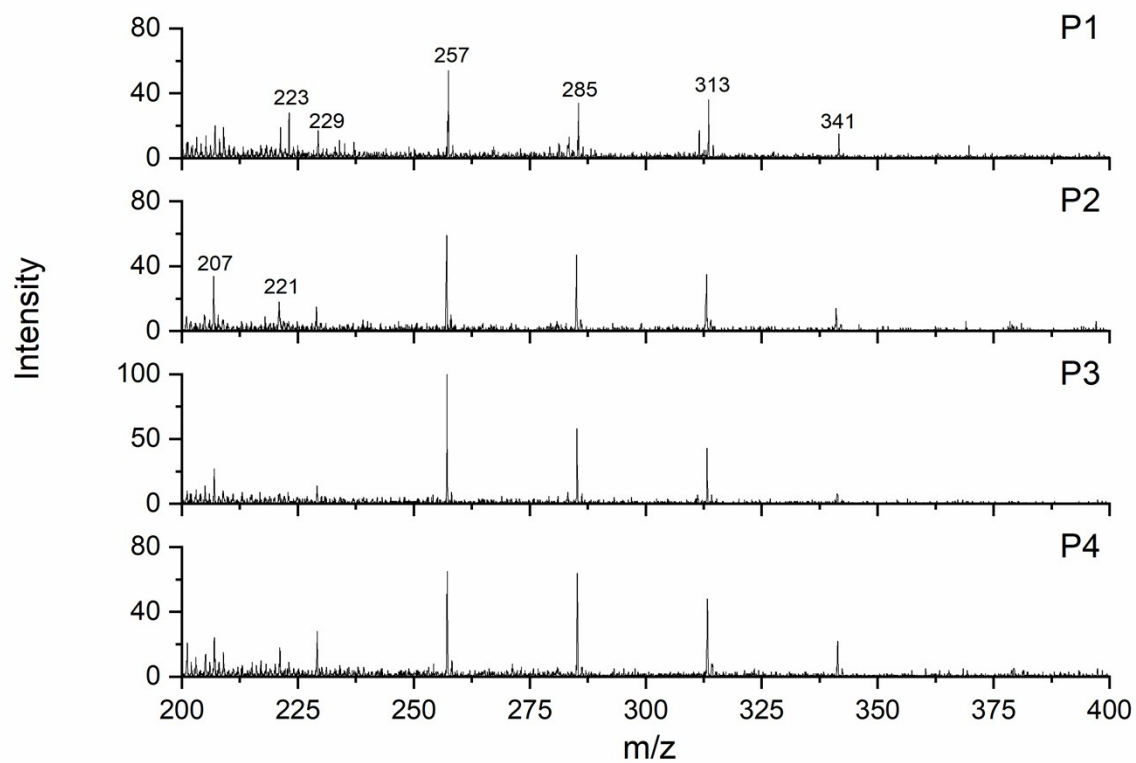


Fig. S4b. ToF-SIMS spectral reproducibility of the DI control seed of the top section in the positive mode (m/z^+ 200 – 400).

P1, P2, P3, and P4 represent the first, second, third, and fourth positive ion mode data acquired consecutively in the DI control seed section.

Supplementary Information

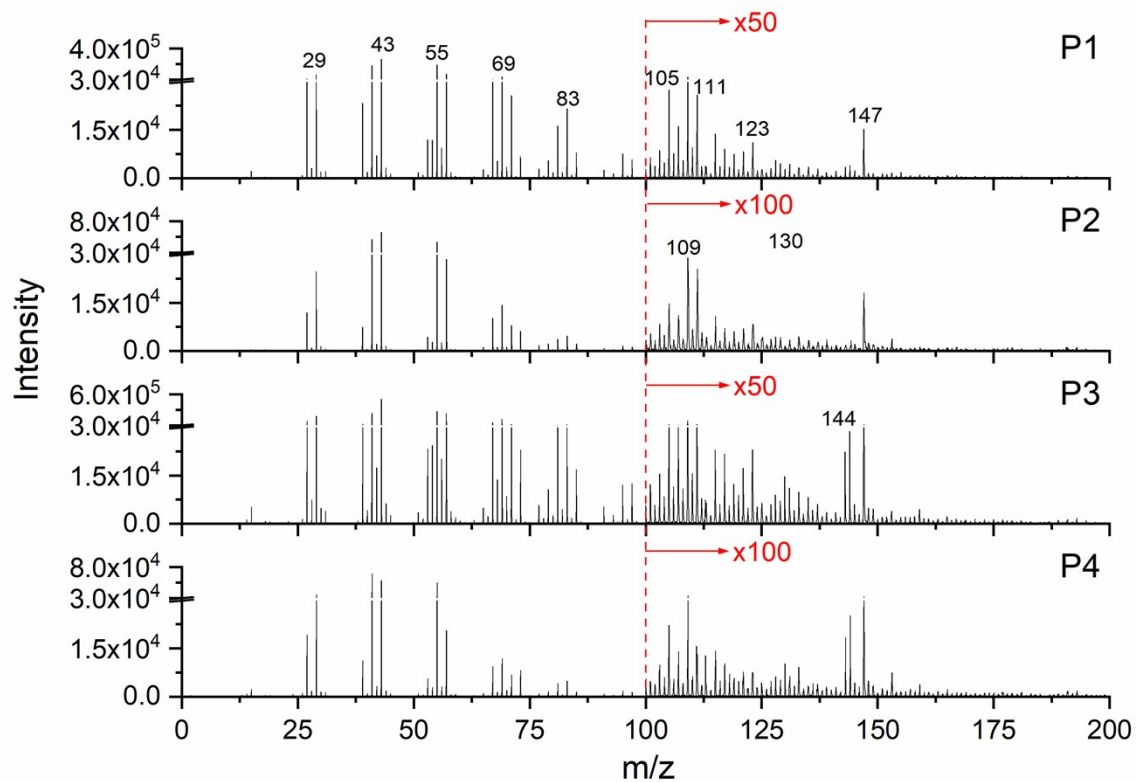


Fig. S5a. ToF-SIMS spectral reproducibility of the DI control seed of the bottom section in the positive mode ($m/z^+ 0 - 200$).

P1, P2, P3, and P4 represent the first, second, third, and fourth positive ion mode data acquired consecutively in the DI control seed section.

Supplementary Information

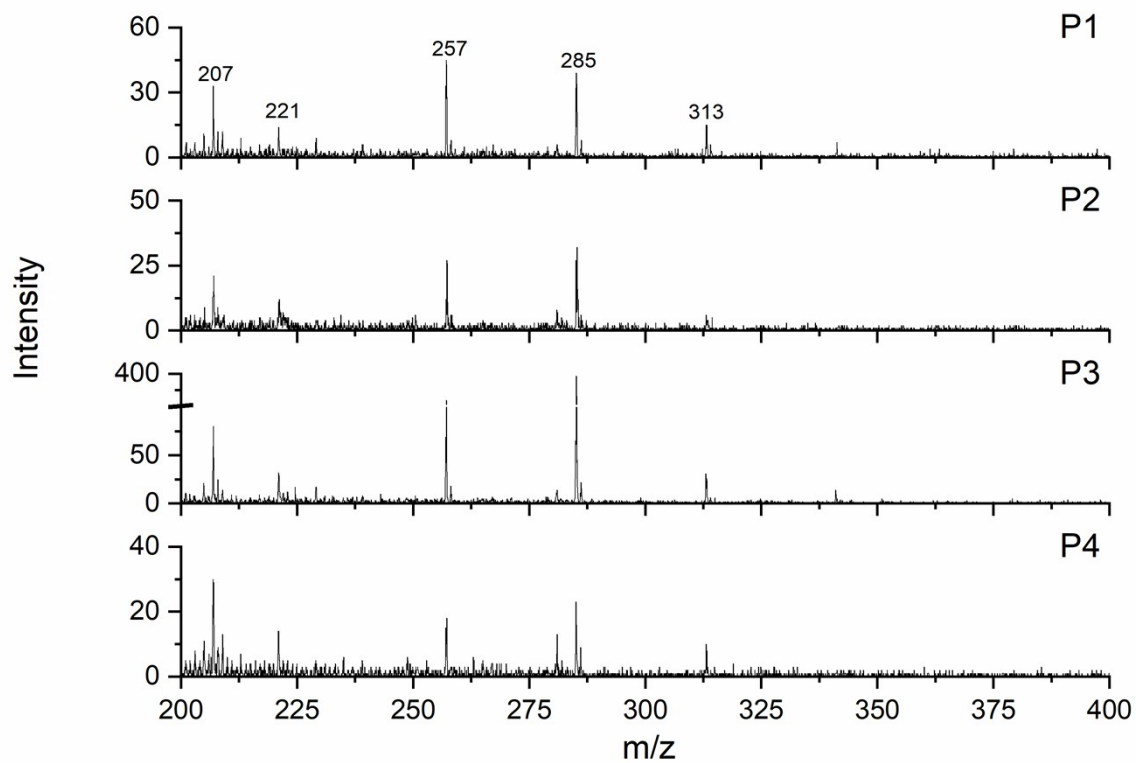


Fig. S5b. ToF-SIMS spectral reproducibility of the DI control seed of the bottom section in the positive mode (m/z^+ 200 – 400).

P1, P2, P3, and P4 represent the first, second, third, and fourth positive ion mode data acquired consecutively in the DI control seed section.

Supplementary Information

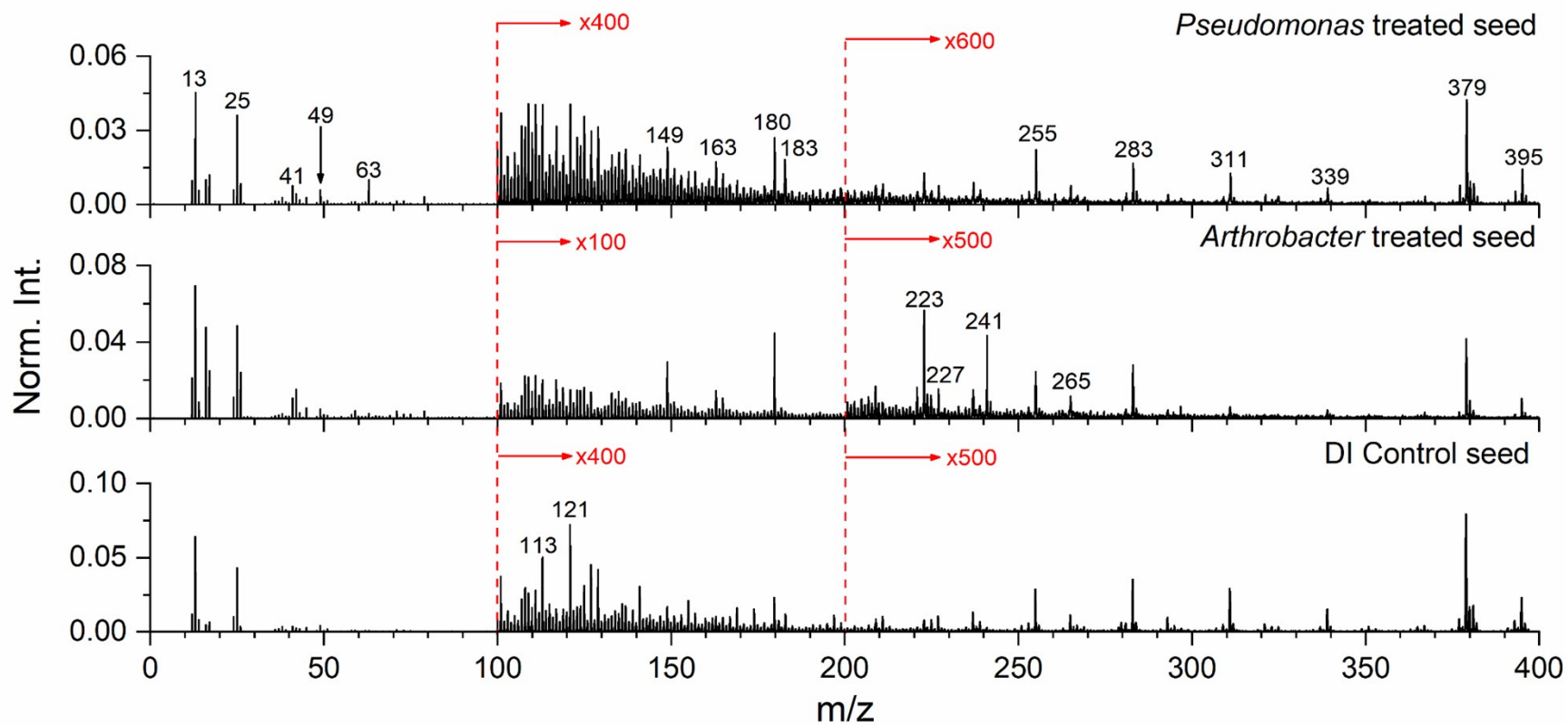


Fig. S6a. ToF-SIMS spectral comparison among three treatments of the top seed sections in the negative mode (m/z 0 – 400). Normalization was done using total ion intensities.

Supplementary Information

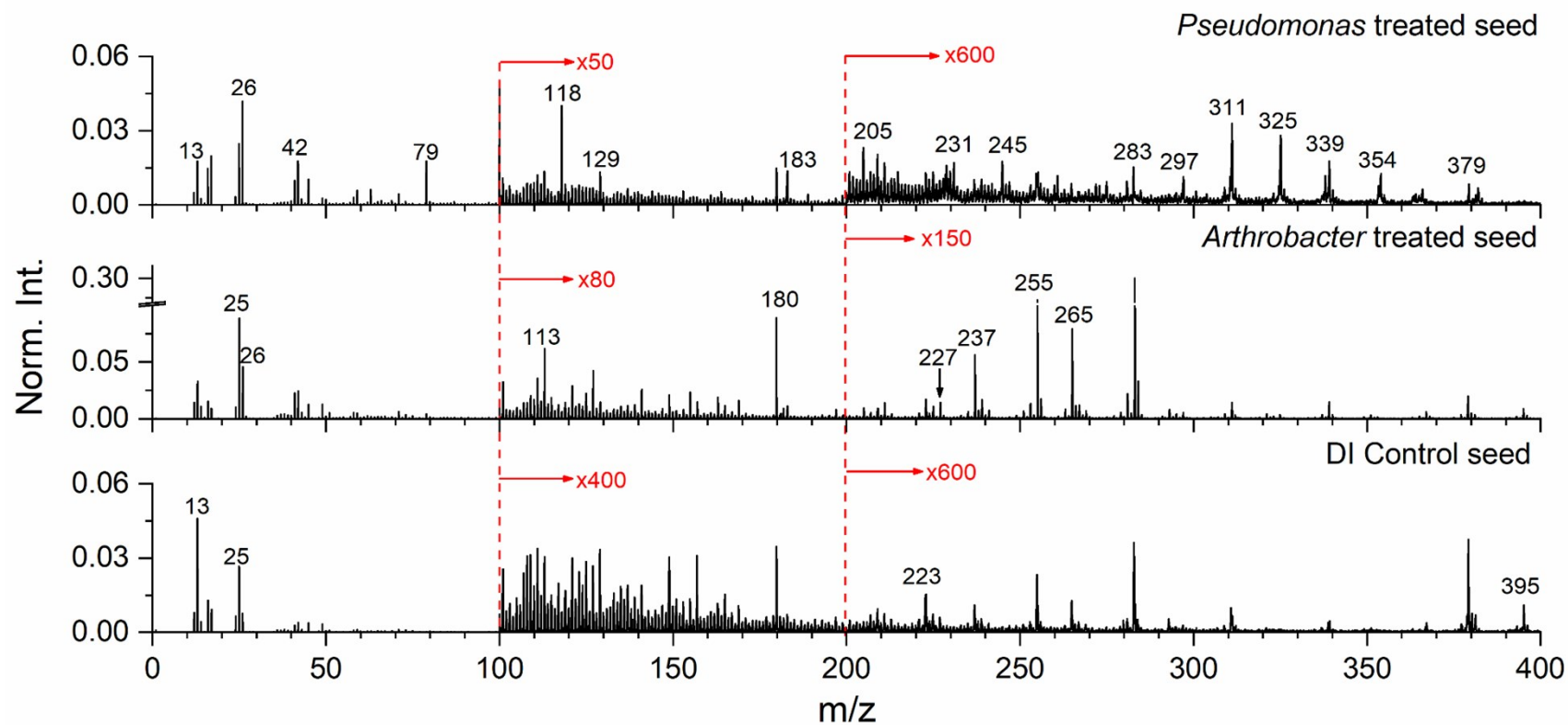


Fig. S6b. ToF-SIMS spectral comparison among three treatments of the bottom seed sections in the negative mode (m/z^- 0 – 400). Normalization was done using total ion intensities.

Supplementary Information

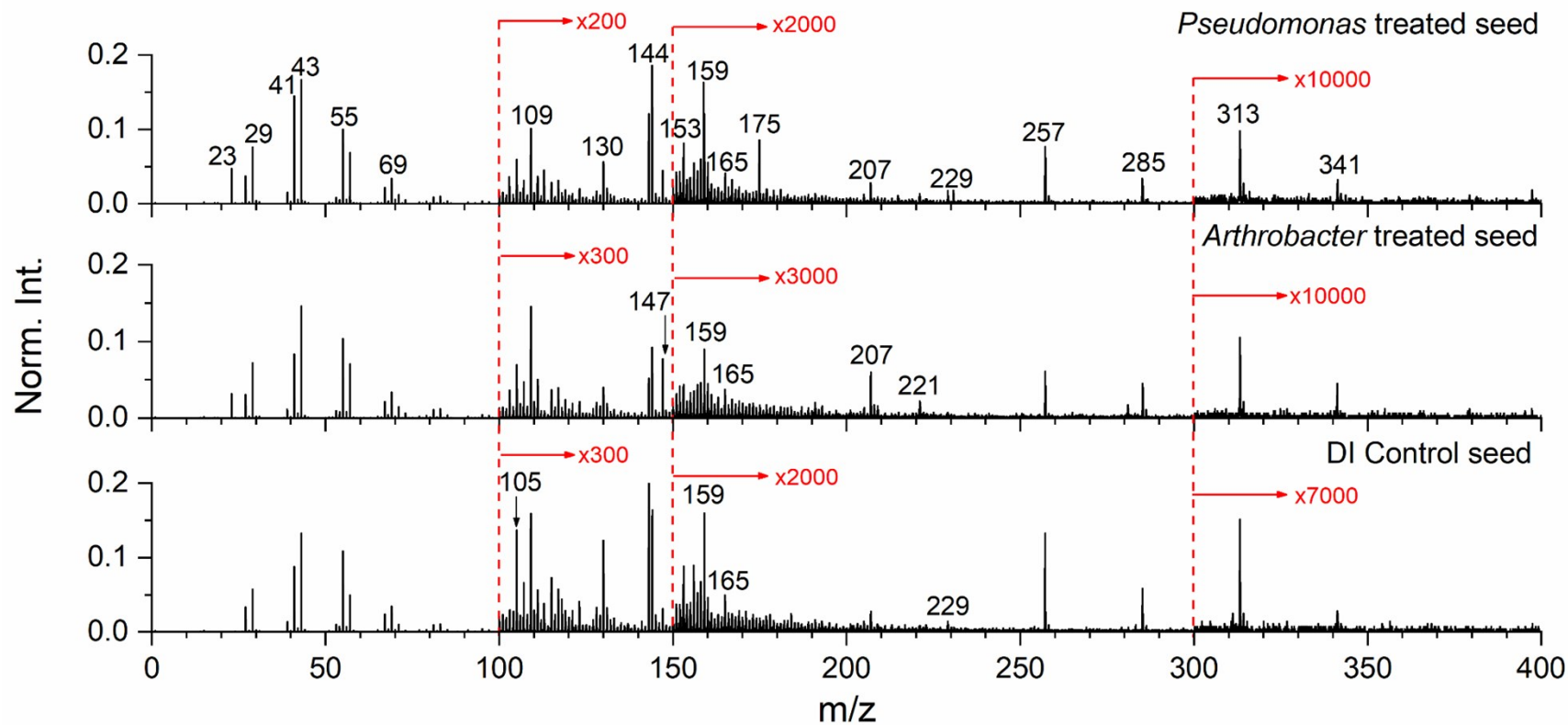


Fig. S7a. ToF-SIMS spectral comparison among three treatments of the top seed sections in the positive mode ($m/z^+ 0 - 400$). Normalization was done using total ion intensities.

Supplementary Information

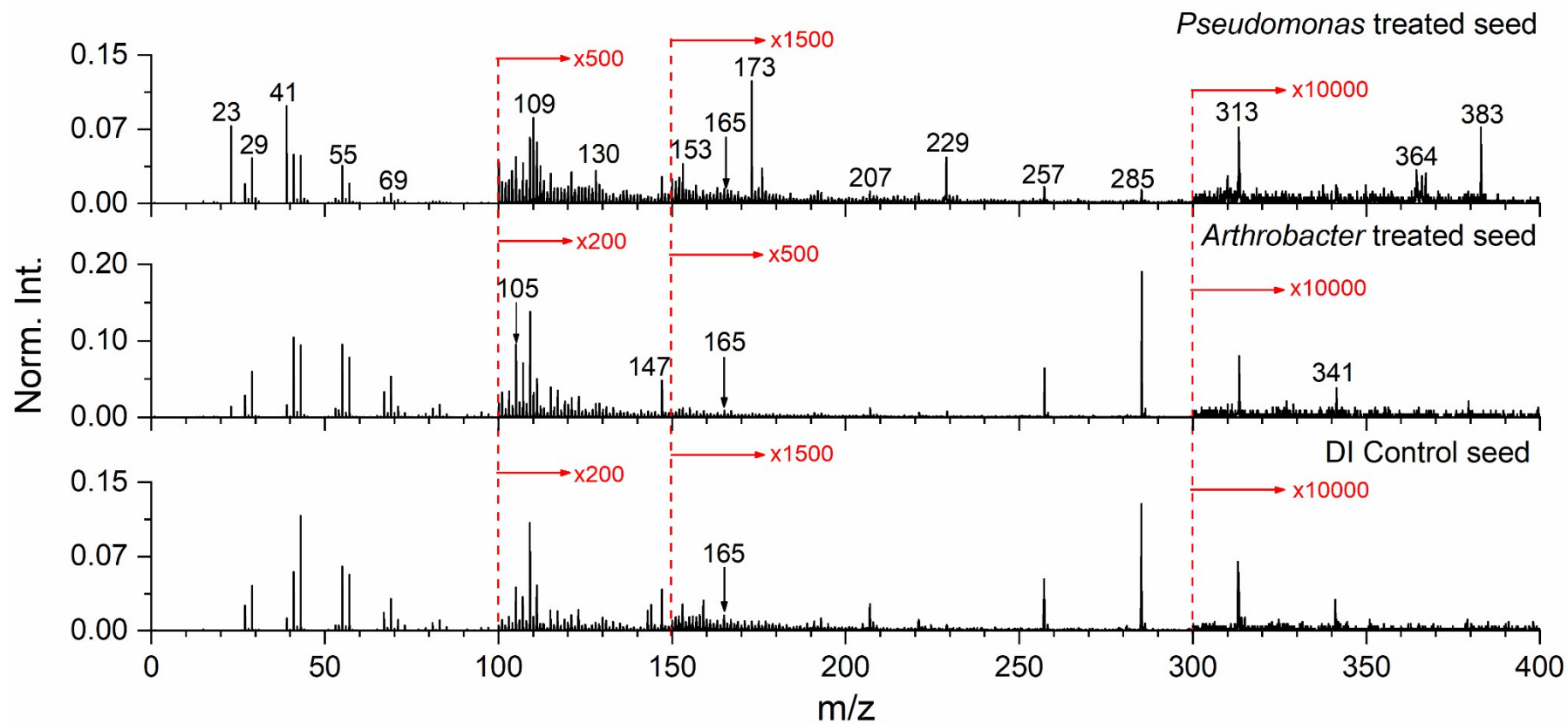


Fig. S7b. ToF-SIMS spectral comparison among three treatments of the bottom seed sections in the positive mode (m/z^+ 0 – 400). Normalization is done using total ion intensities.

Supplementary Information

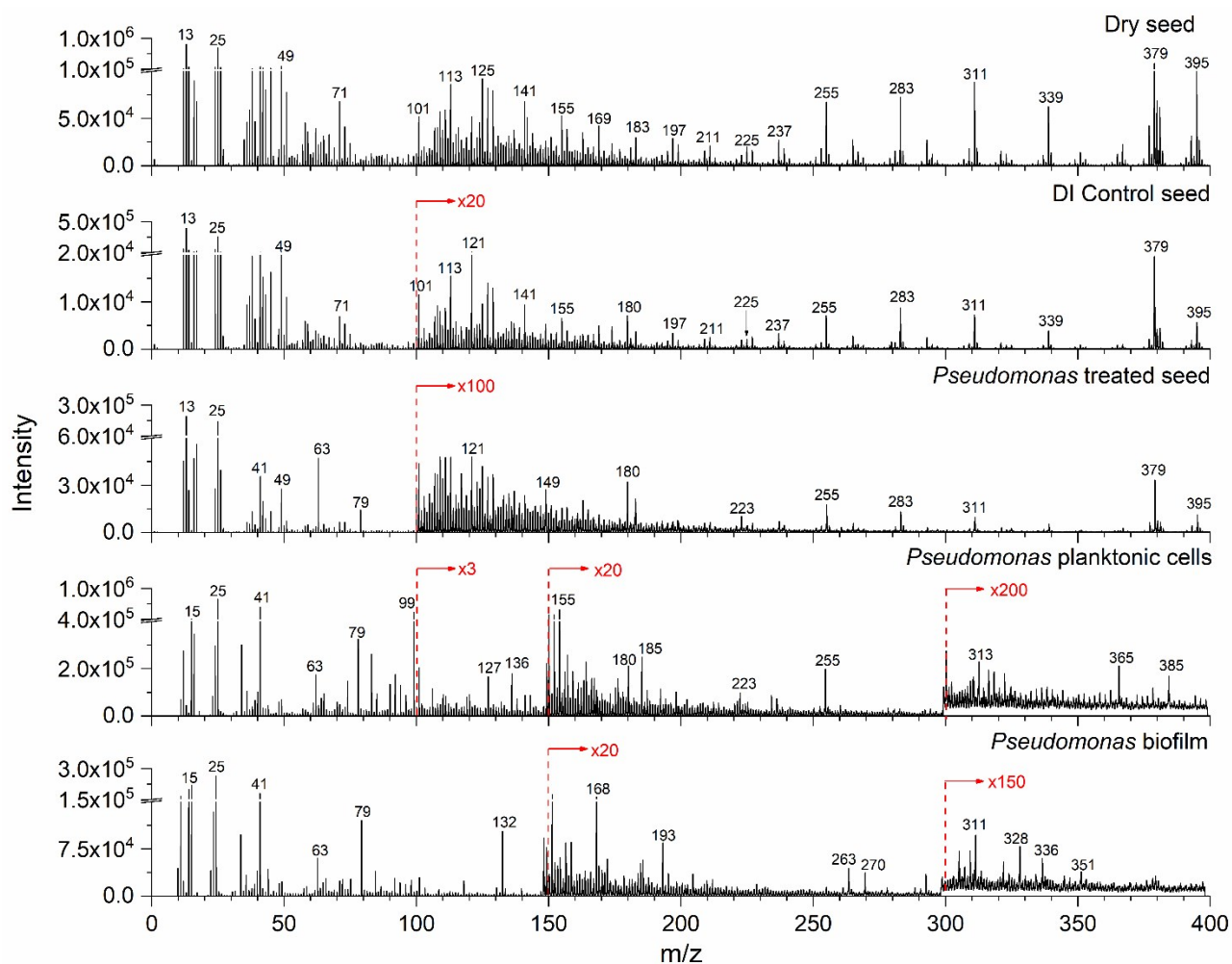


Fig. S8a. ToF-SIMS spectral comparison of the top section of the dry seed, DI control seed, *P.*-treated seed, and the *P.*-bacteria control in the negative mode (m/z^- 0 – 400).

Figure S8a depicts ToF-SIMS spectral results of the top section of the *Brachypodium* seed with and without bacteria treatment.

Supplementary Information

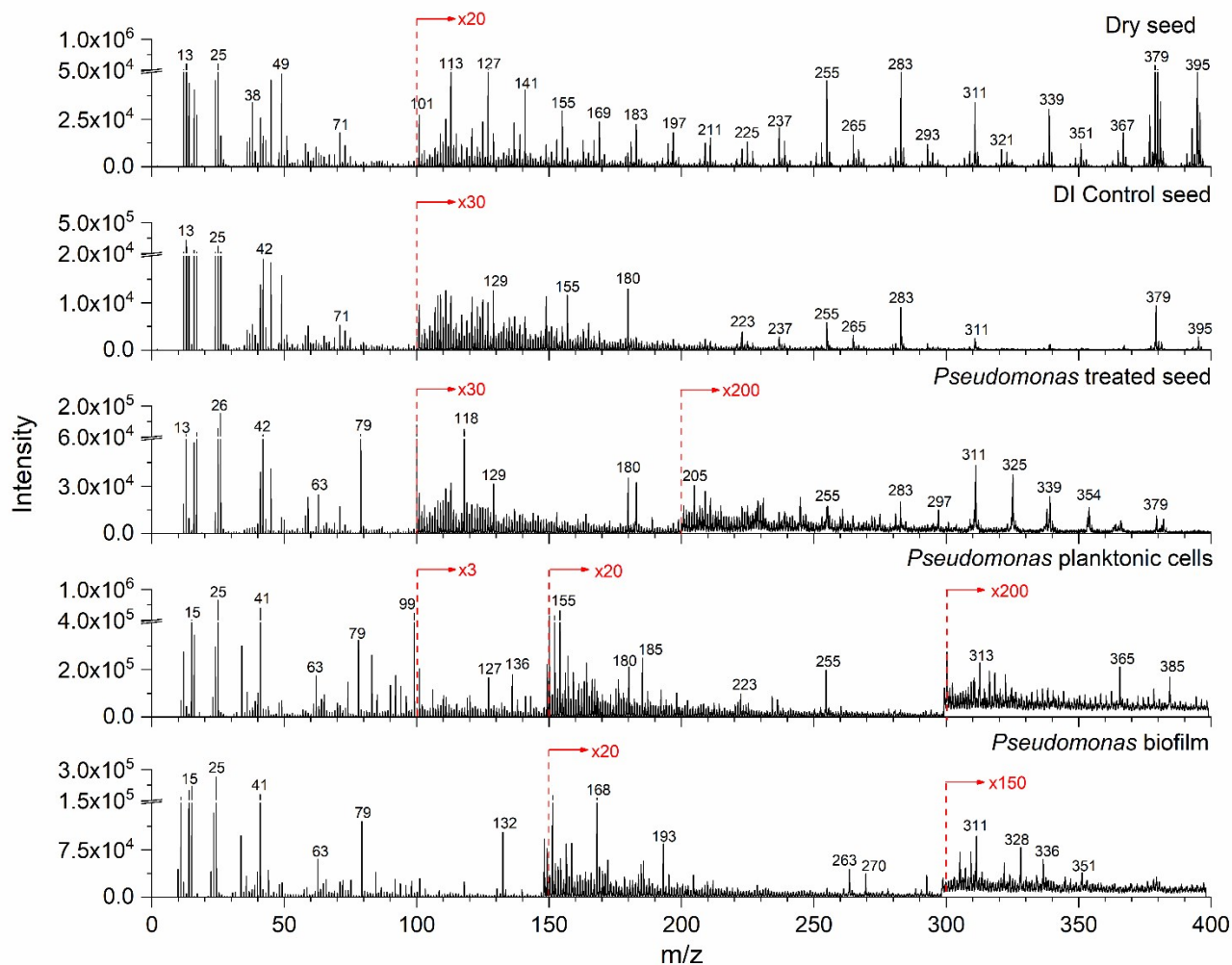


Fig. S8b. ToF-SIMS spectral comparison of the bottom section of the dry seed, DI control seed, *P.*-treated seed, and the *P.*-bacteria control in the negative mode (m/z^- 0 – 400).

Figure S8b depicts ToF-SIMS spectral results of the bottom section of the *Brachypodium* seed with and without bacteria treatment.

Supplementary Information

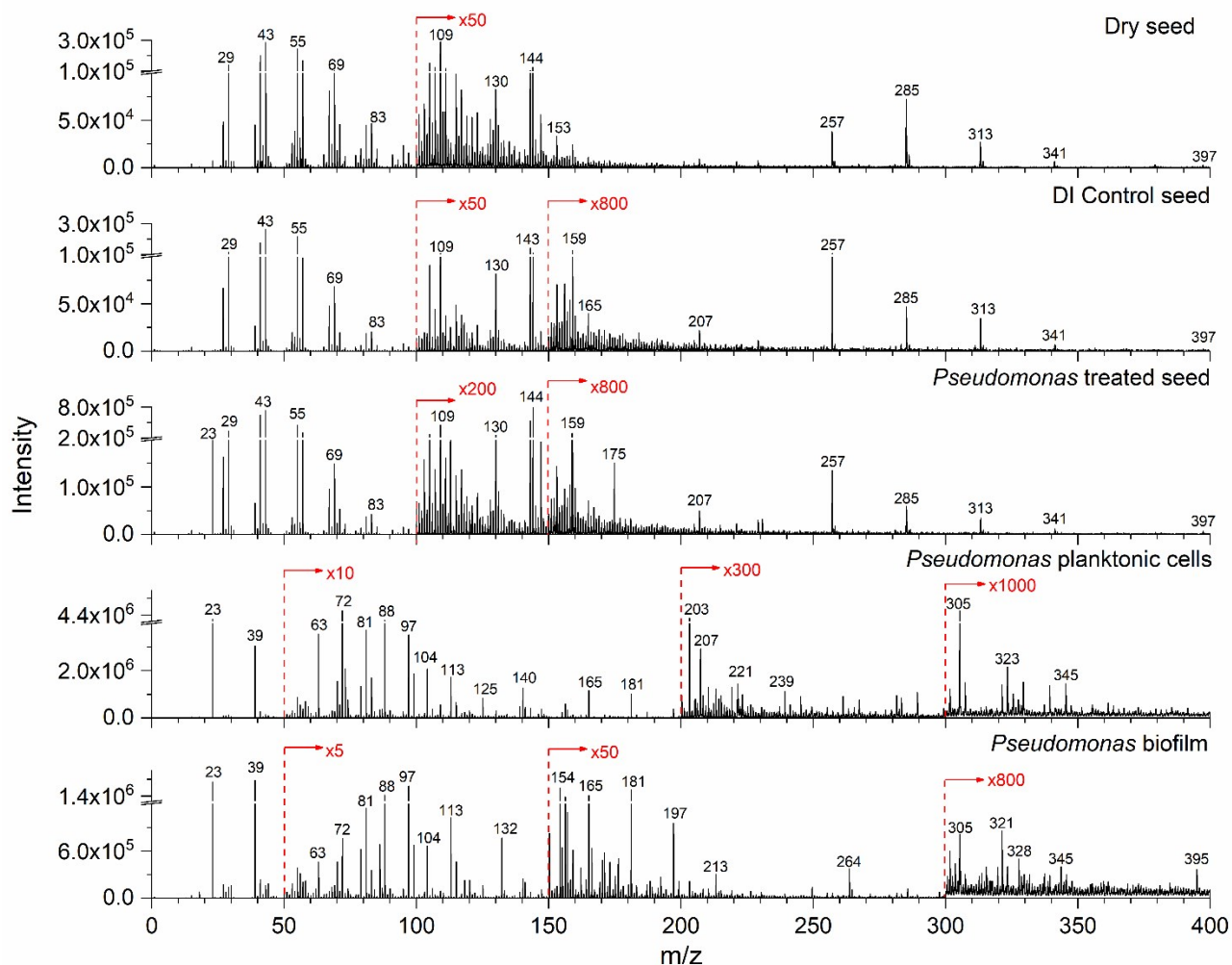


Fig. S9a. ToF-SIMS spectral comparison of the top section of the dry seed, DI control seed, *P.*-treated seed, and the *P.*-bacteria control in the positive mode (m/z^+ 0 – 400).

Figure S9a depicts ToF-SIMS spectral results of the top section of the *Brachypodium* seed with and without bacteria treatment.

Supplementary Information

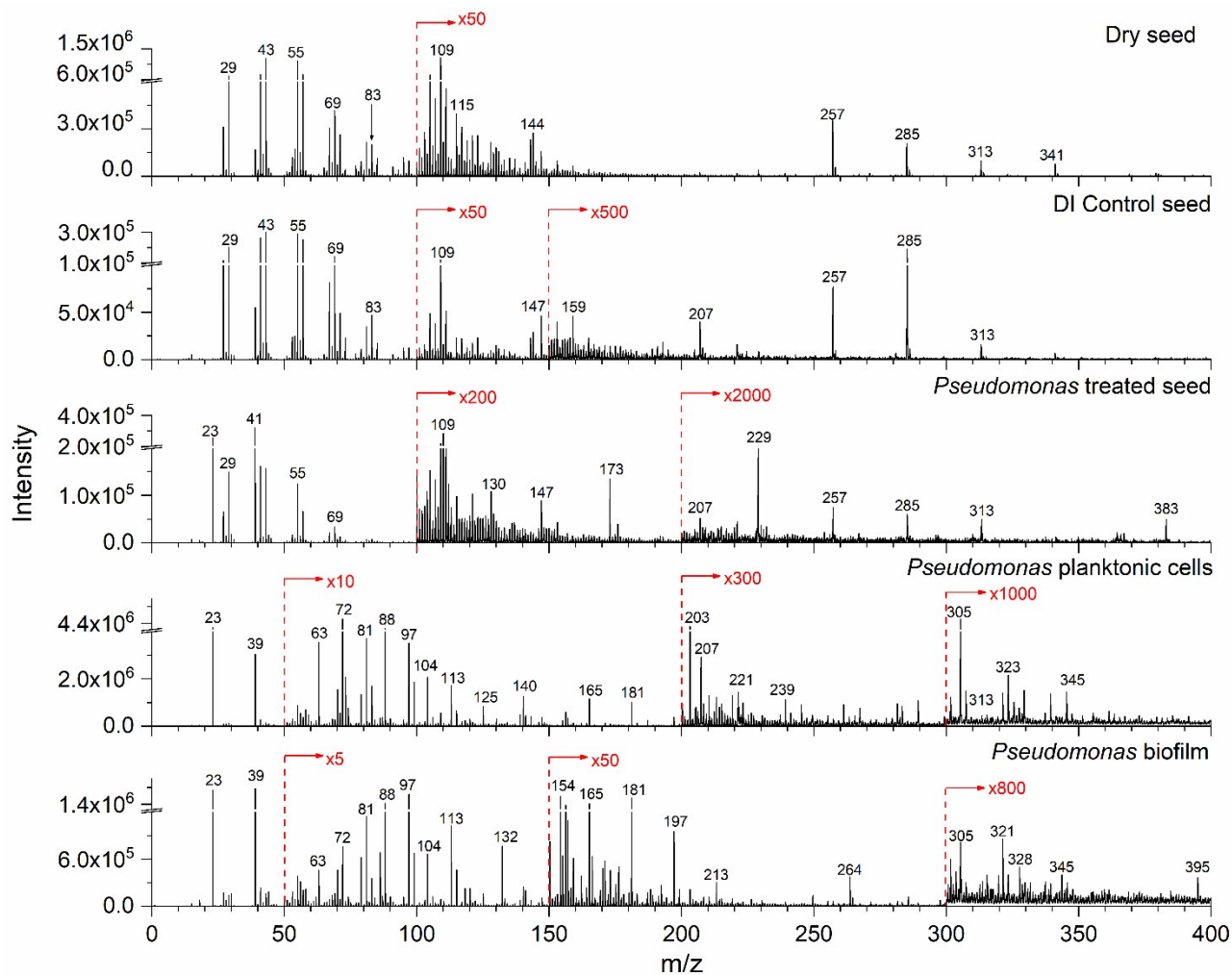


Fig. S9b. ToF-SIMS spectral comparison of the bottom section of the dry seed, DI control seed, *P.*-treated seed, and the *P.*-bacteria control in the positive mode ($m/z^+ 0 - 400$).

Figure S9b depicts ToF-SIMS spectral results of the bottom section of the *Brachypodium* seed with and without bacteria treatment.

Supplementary Information

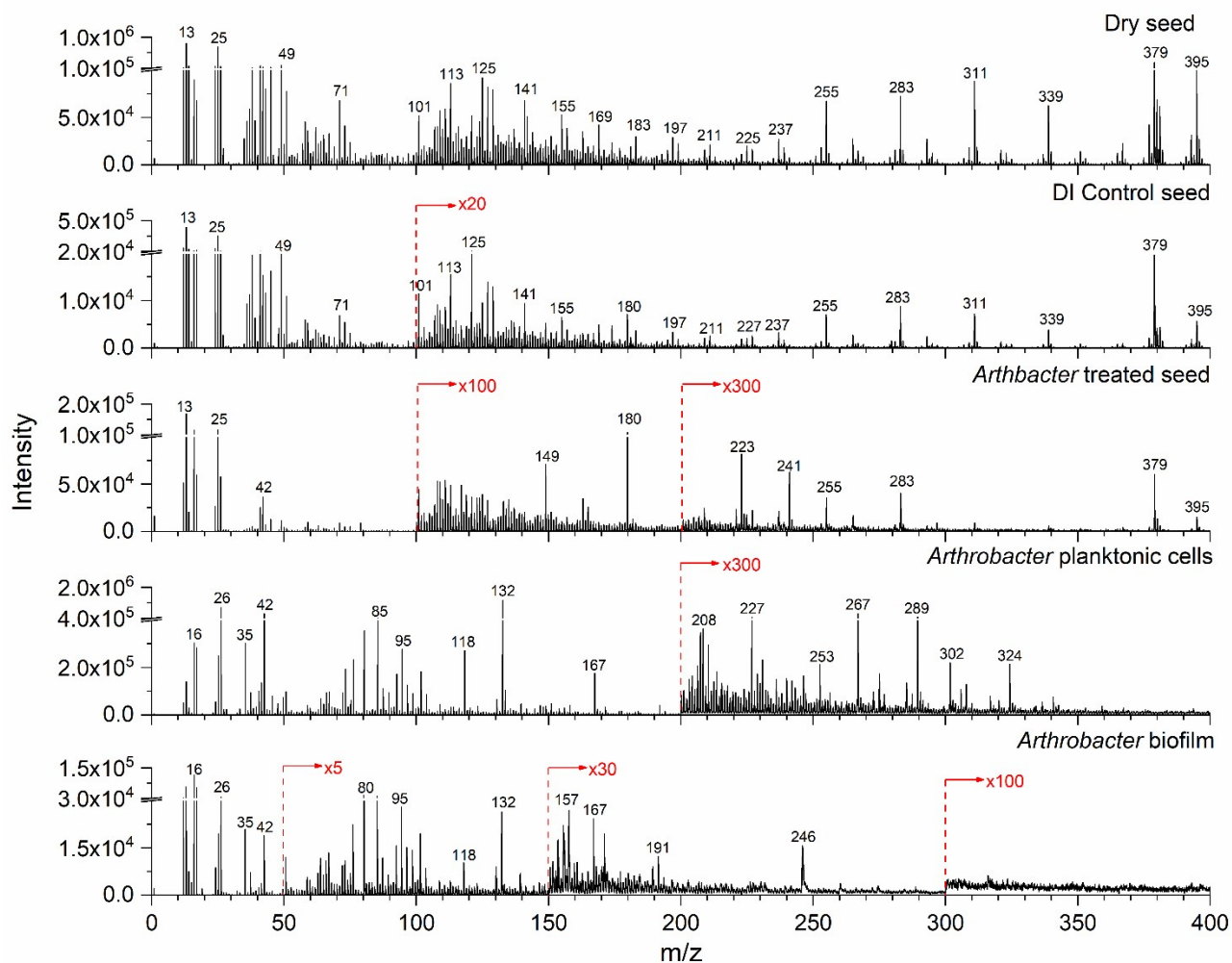


Fig. S10a. ToF-SIMS spectral comparison of the top section of the dry seed, DI control seed, *A.*-treated seed, and the *A.*-bacteria control in the negative mode (m/z^- 0 – 400).

Fig. S10a depicts ToF-SIMS spectral results of the bottom section of the *Brachypodium* seed with and without bacteria treatment.

Supplementary Information

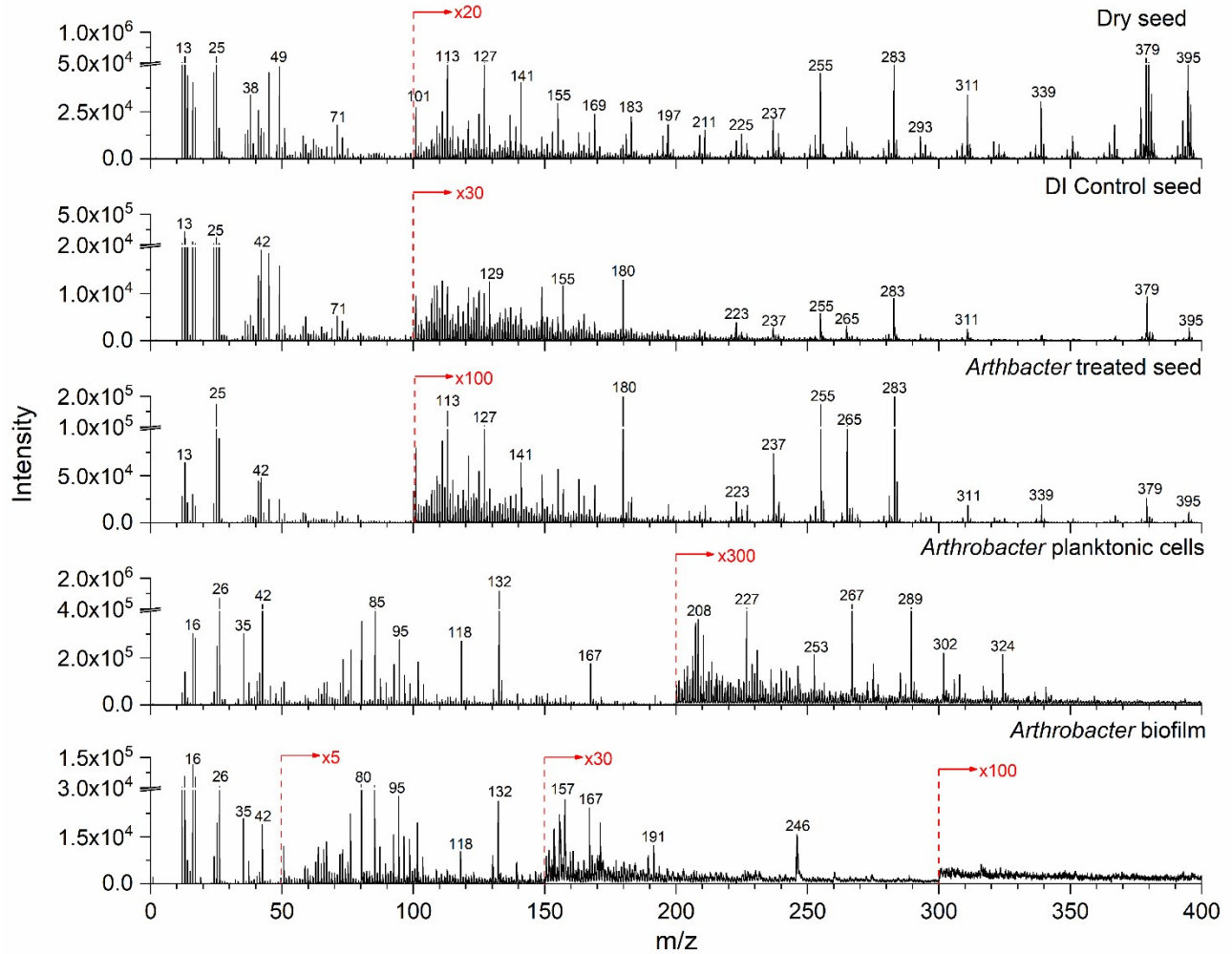


Fig. S10b. ToF-SIMS spectral comparison of the bottom section of the dry seed, DI control seed, *A.*-treated seed, and the *A.*-bacteria control in the negative mode ($m/z^- 0 - 400$).

Figure S10b depicts ToF-SIMS spectral results of the bottom section of the *Brachypodium* seed with and without bacteria treatment.

Supplementary Information

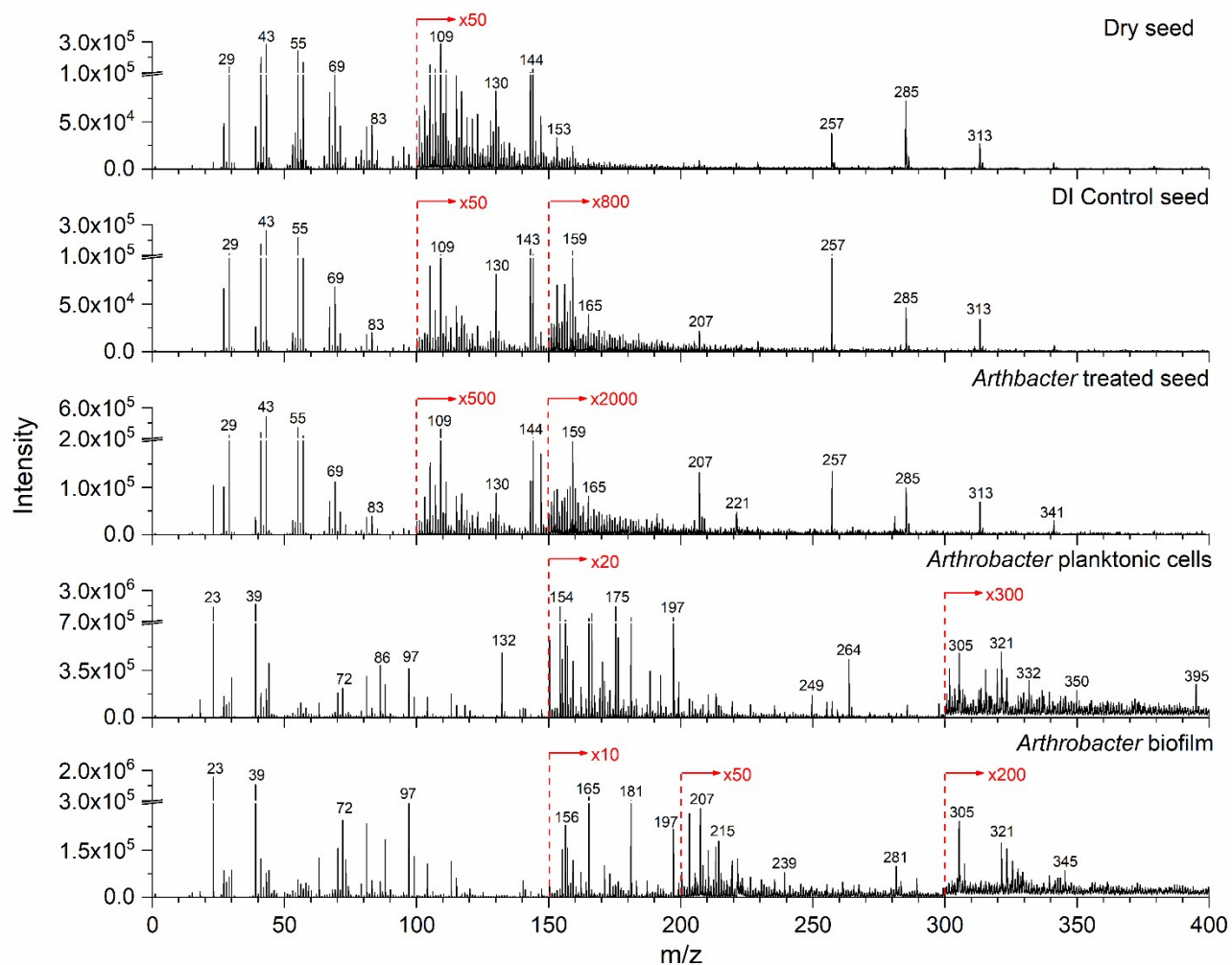


Fig. S11a. ToF-SIMS spectral comparison in the top section of the dry seed, DI control seed, *A.*-treated seed, and the *A.*-bacteria control in the positive mode (m/z^+ 0 – 400).

Figure S11a depicts ToF-SIMS spectral results of the bottom section of the *Brachypodium* seed with and without bacteria treatment.

Supplementary Information

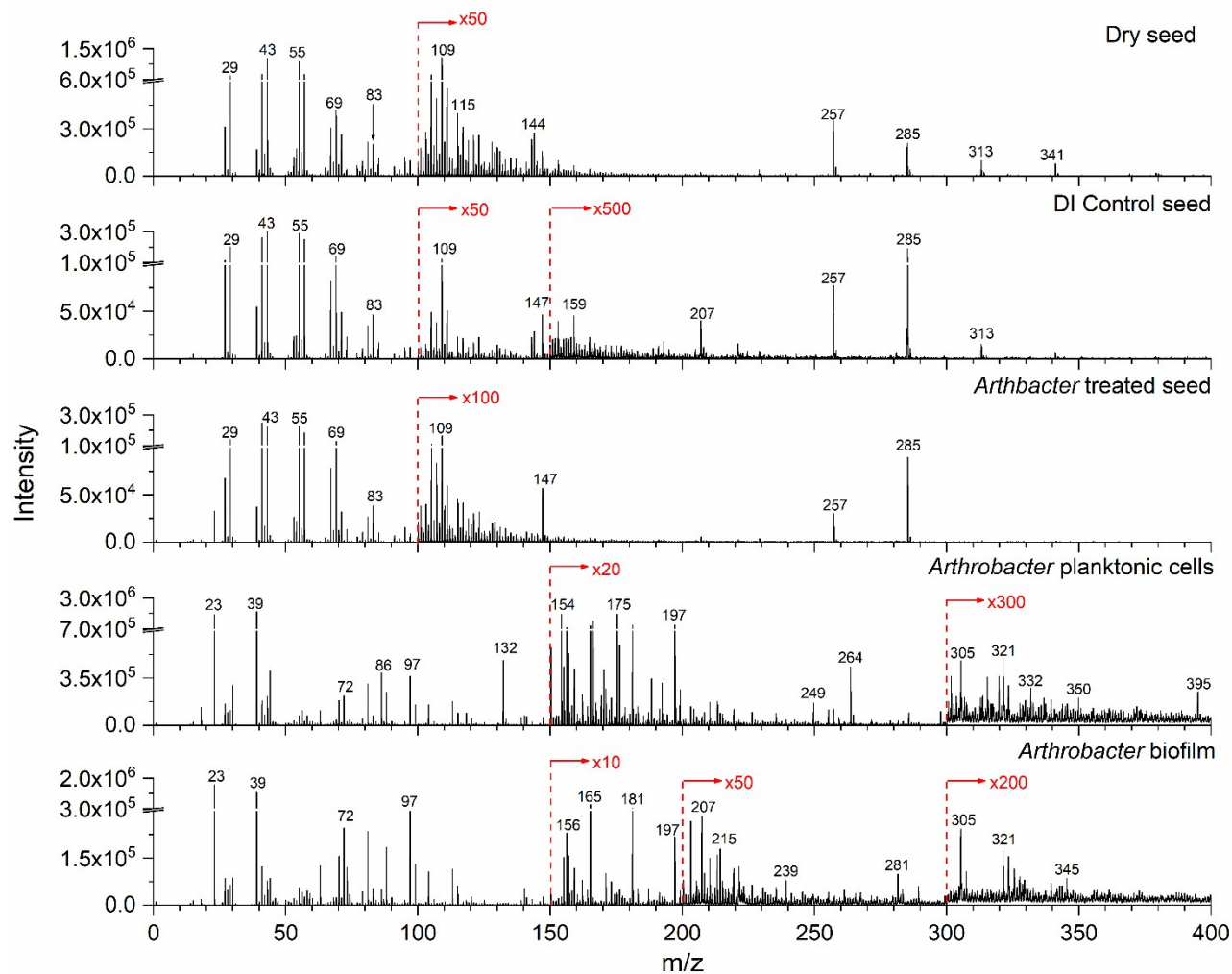


Fig. S11b. ToF-SIMS spectral comparison in the bottom section of the dry seed, DI control seed, *A.*-treated seed, and *A.*-bacteria control seed in the positive mode ($m/z^+ 0 - 400$).

Figure S11b depicts ToF-SIMS spectral results of the bottom section of the *Brachypodium* seed with and without bacteria treatment.

Supplementary Information

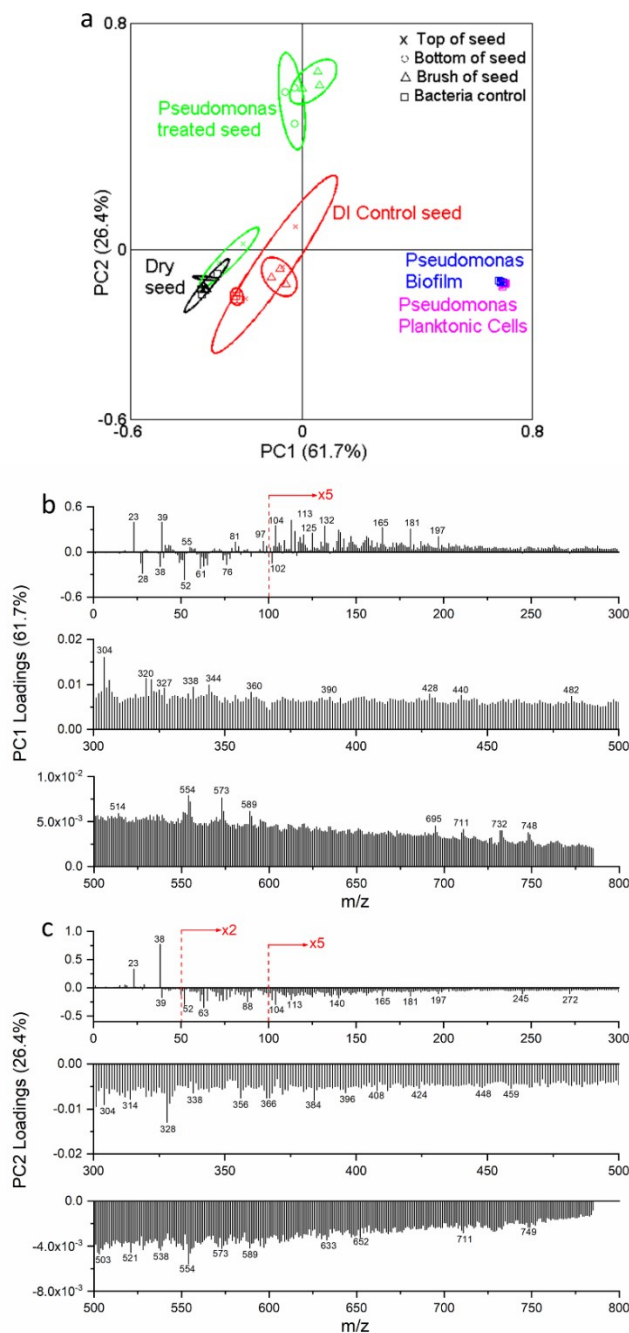


Fig. S12. All peak spectral PCA results: (a) PC1 and PC2 scores plot, (b) PC1 loadings plot, and (c) PC2 loadings plot of *P.*-treated samples in the positive mode ($m/z^+ 0 - 800$).

In the PC1 vs. PC2 scores plot shown in Fig. S12, different symbols represent different seed sections. The black color represents dry seed, red color DI water control, green *Pseudomonas* treated seed, blue *Pseudomonas* biofilm, and magenta *Pseudomonas* planktonic cells. PC1 explains 61.7% of all data, and it mainly separates the DI control seed, different sections of the dry seed, DI control seed and the *P.*-treated seed from the *P.* bacteria control samples, including *P.* planktonic cells and biofilms. PC2 explains 26.4 % of all data, and it mainly separates the dry seed, DI control seed, top of the *P.*-treated seed and *P.* bacteria control samples from the bottom and brush sections of the *P.*-treated seed.

Supplementary Information

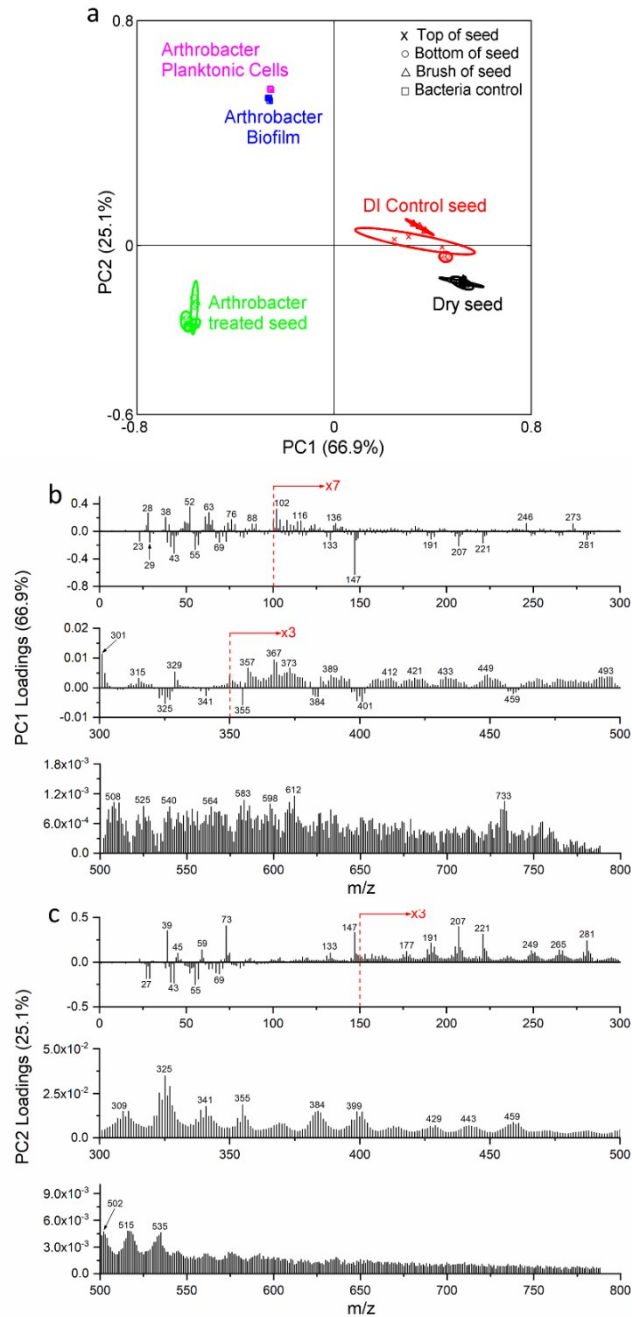


Fig. S13. All peak spectral PCA results: (a) PC1 and PC2 scores plot, (b) PC1 loadings plot, and (c) PC2 loadings plot of *A.*-treated samples in the positive mode ($m/z^+ 0 - 800$).

In the PC1 vs. PC2 scores plot shown in Fig. S13, different symbols represent different seed sections. The black color represents dry seed, red color DI water control, green *Arthrobacter* treated seed, blue *Arthrobacter* biofilm, and magenta *Arthrobacter* planktonic cells. PC1 explains 66.9% of all data, and it mainly separates the dry seed and DI control seed from the *A.* treated seed and *A.* bacteria control samples, including *A.* planktonic cells and biofilms. PC2 explains 25.1% of all data, and it mainly separates the dry seed, top to bottom sections of the DI control seed and the *A.*-treated seed from the brush section of the DI control seed and *A.* bacteria control samples.

Supplementary Information

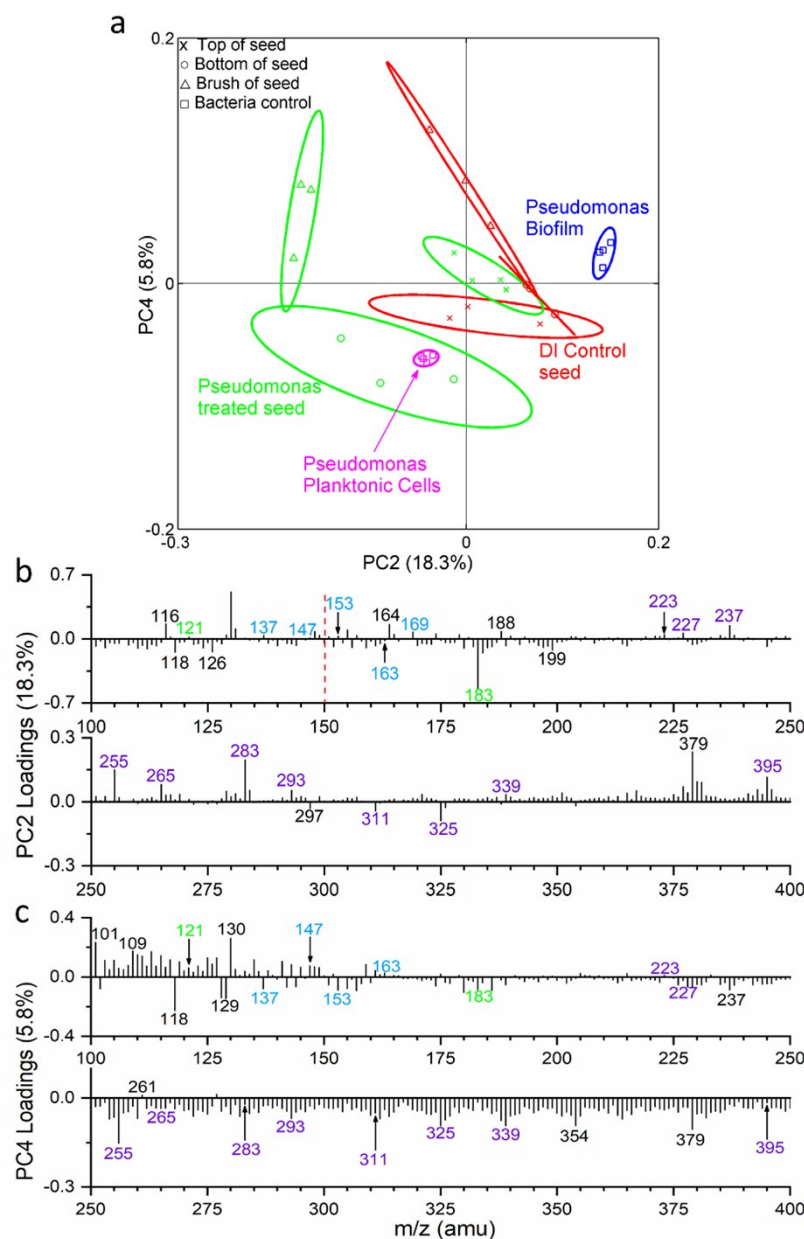


Fig. S14. Selected peak spectral PCA results: (a) PC2 and PC4 scores plot, (b) PC2 loadings plot, and (c) PC4 loadings plot of *P.*-treated samples in the negative mode (m/z^- 100 – 400).

In the scores plot of PC2 vs. PC4 shown in Fig. S14, different symbols represent different seed sections. Red color indicates DI water control, green *Pseudomonas* treated seed, blue *Pseudomonas* biofilm, and magenta *Pseudomonas* planktonic cells. Peaks are labelled with their center masses. Peaks colored in green, blue, and purple represent flavonoid fragments, phenolic acids, and fatty acids, respectively. PC2 explains 18.3 % of all data, and PC2 positive shows overlaps between the *P.* biofilm and the top of the *P.*-treated seed; whereas PC2 negative gives similarities among *P.* planktonic cells and the bottom and brush of the *P.*-treated seed. PC4 explains 5.8% of data, however, PC4 positive is more representative of the *P.* bacterial biofilm and the PC4 negative *P.* planktonic cells. Additionally, PC4 separates different sections of the *P.*-treated seed.

Supplementary Information

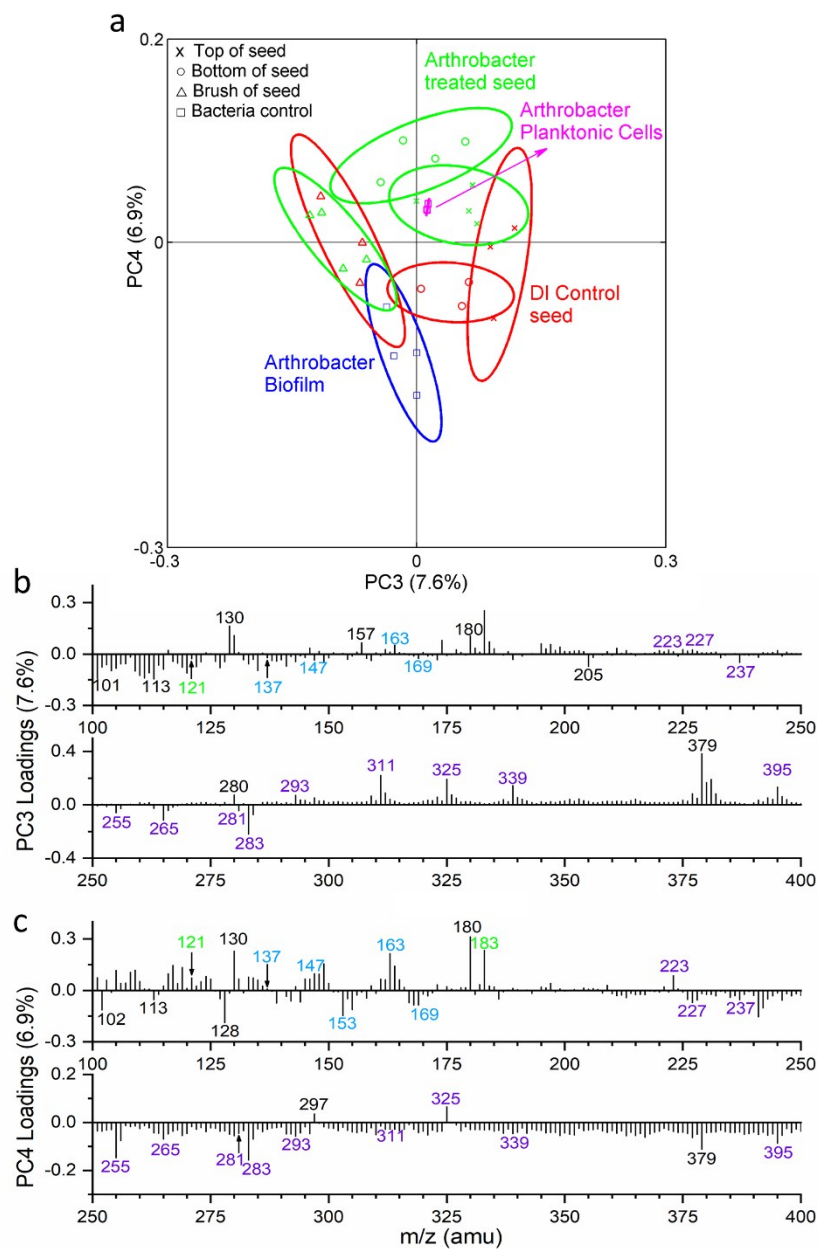


Fig. S15. Selected peak spectral PCA results: (a) PC3 and PC4 scores plot, (b) PC3 loadings plot, and (c) PC4 loadings plot of *A.*-treated samples in the negative mode (m/z^- 100 – 400).

In the PC3 vs. PC4 scores plot shown in Fig. S15, different symbols represent different seed sections. Red color indicates DI water control, green *Arthrobacter* treated seed, blue *Arthrobacter* biofilm, and magenta *Arthrobacter* planktonic cells. Peaks are labelled with their center masses. Peaks colored in green, blue, and purple represent flavonoid fragments, phenolic acids, and fatty acids, respectively. PC3 explains 7.6% of all data, and PC3 positive is more representative of *A.* planktonic cells and PC3 negative *A.* biofilms. PC4 explains 6.9% of all data. PC4 positive shows overlaps among the top, bottom, and part of the brush of the *A.*-treated seed. PC4 negative shows similarities between the brush and the *A.*-biofilm.

Supplementary Information

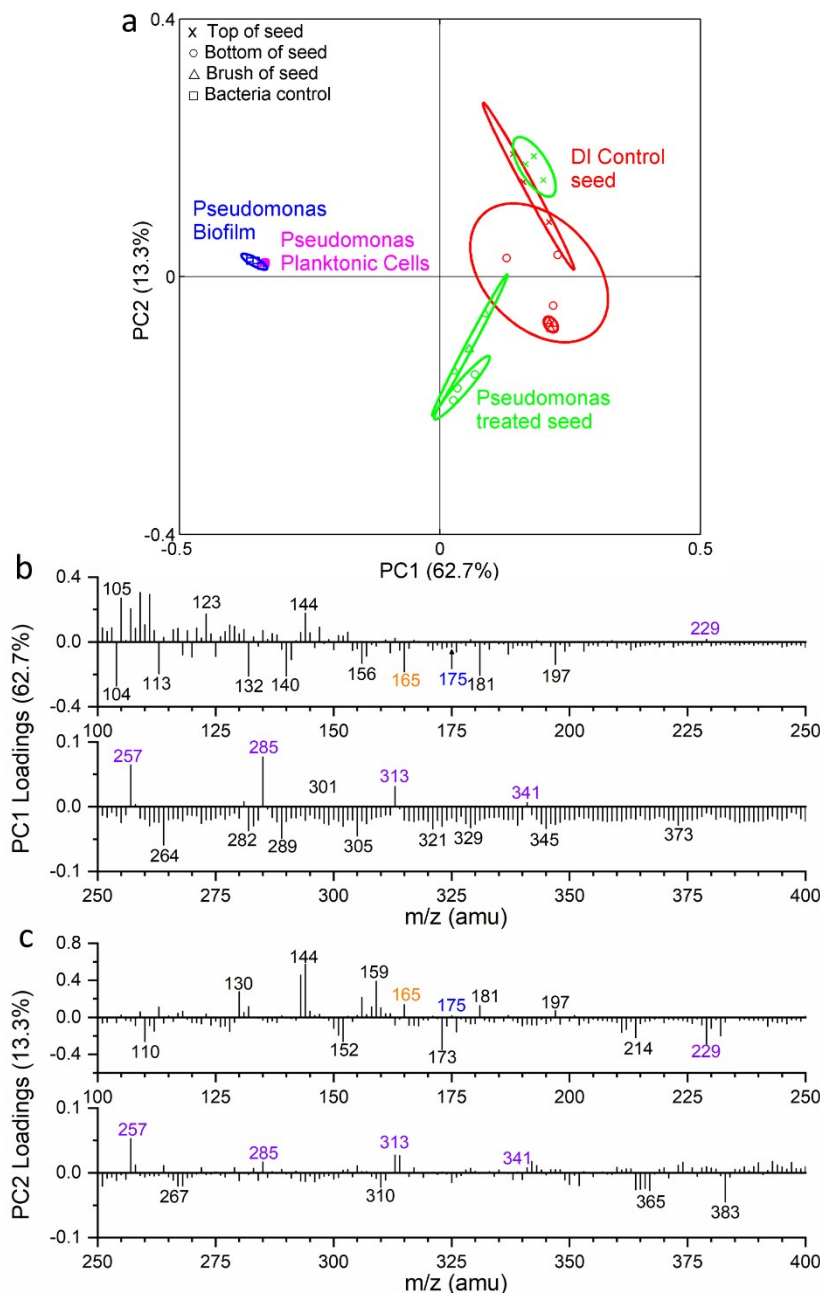


Fig. S16. Selected peak spectral PCA results: (a) PC1 and PC2 scores plot, (b) PC1 loadings plot, and (c) PC2 loadings plot of *P.*-treated samples in the positive mode ($m/z^+ 100 - 400$).

Different symbols represent different seed sections in the PC1 vs. PC2 scores plot in Fig. S16. Red color indicates DI water control, green *Pseudomonas* treated seed, blue *Pseudomonas* biofilm, and magenta *Pseudomonas* planktonic cells. Peaks are labelled with their center masses. α -tocopherol fragment peak label is colored in orange, IAA peak label blue, and fatty acids peaks purple in the loadings plots. Peaks are labelled in their center masses.

PC1 explains 62.7% of data and separates the *P.* bacteria controls from the DI control seed and *P.*-treated seed. PC2 explains 13.3% of data and separates the brush segment of the DI control seed and the bottom to brush sections of the *P.*-treated seed from other samples.

Supplementary Information

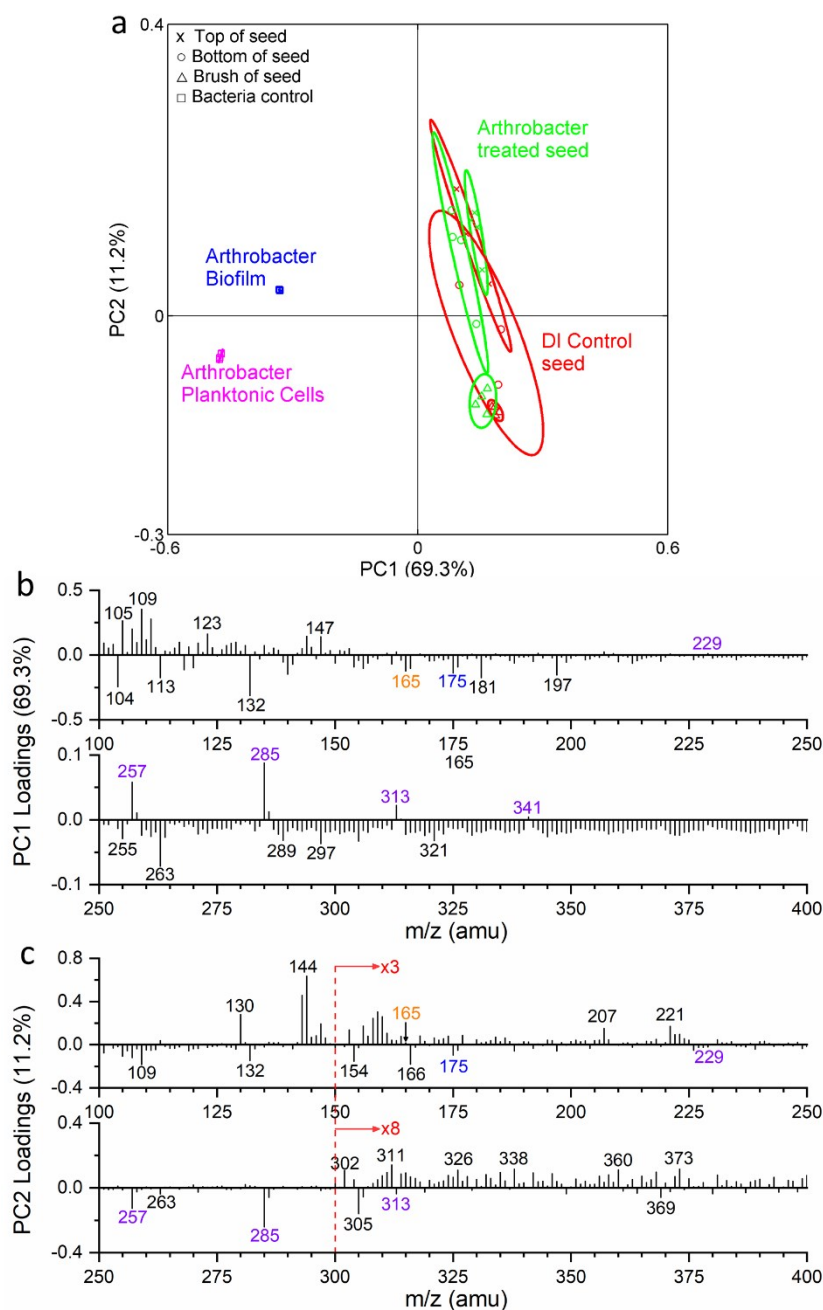


Fig. S17. Selected peak spectral PCA results: (a) the PC1 and PC2 scores plot, (b) PC1 loadings plot, and (c) PC2 loadings plot of *A.*-treated samples in the positive mode ($m/z^+ 100 - 400$).

Different symbols represent different seed sections in the PC1 vs. PC2 scores plot in Fig. S17. Red color indicates DI water control, green *Arthrobacter* treated seed, blue *Arthrobacter* biofilm, and magenta *Arthrobacter* planktonic cells. Peaks are labelled with their center masses. α -tocopherol fragment peak label is colored in orange, IAA peak label blue, and fatty acids peaks purple in the loadings plots. Peaks are labelled in their center masses. PC1 captures 69.3% of the variance and distinguishes the *A.* bacteria controls from the DI control seed and *A.*-treated seed. PC2 captures 11.2% of the variance and distinguishes the brush segments of the DI control seed, the *A.*-treated seed, and *A.* planktonic cells from other samples.

Supplementary Information

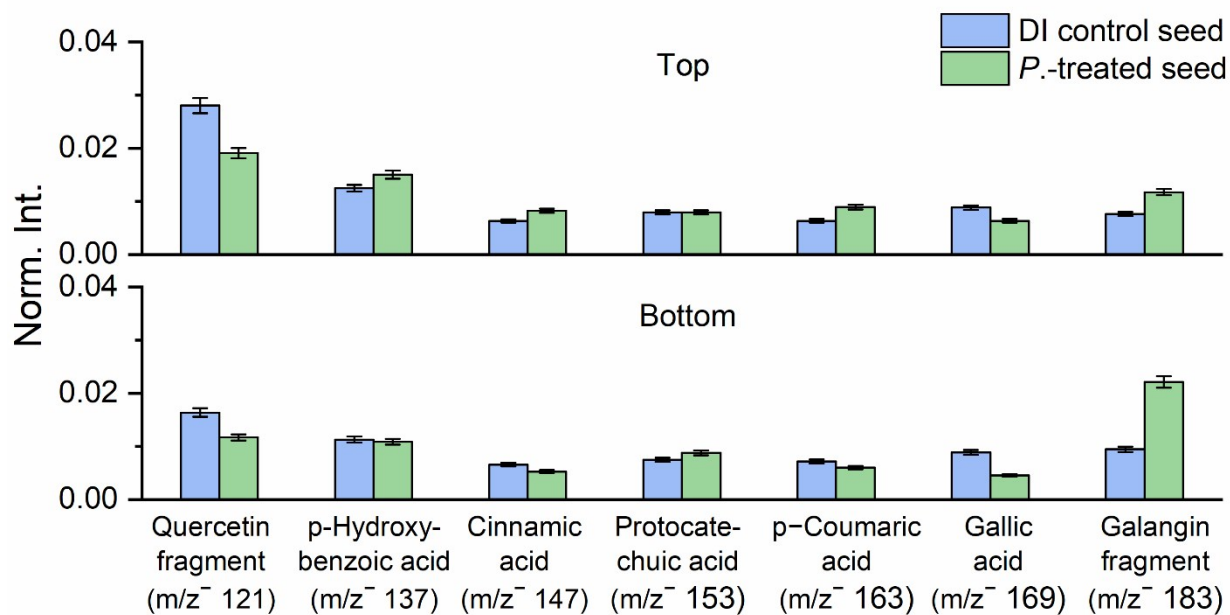


Fig. S18. The normalized comparison bar plots between the DI control seed and *P.*-treated seed in the negative ion mode (m/z^- 100 – 400).

Mean values of multiple replicate measurements are used in the bar plots. Error bars represent standard deviations ($n \geq 3$).

Supplementary Information

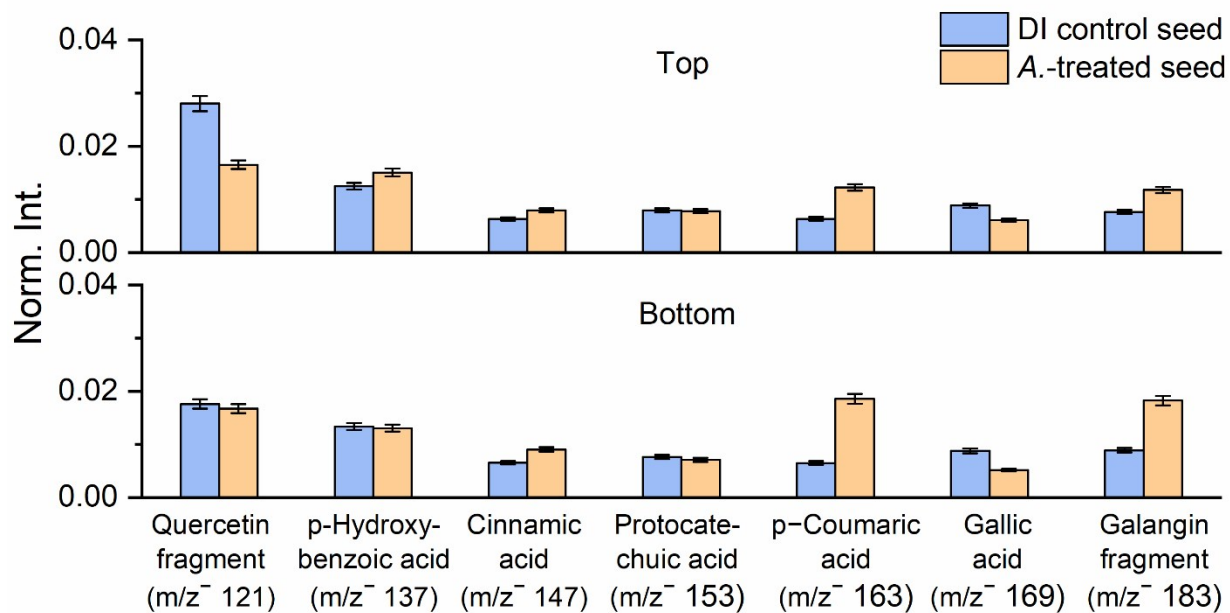


Fig. S19. The normalized comparison bar plots between the DI control seed and *A.*-treated seed in the negative ion mode (m/z^- 100 – 400).

Mean values of multiple replicate measurements are used in the bar plots. Error bars represent standard deviations ($n \geq 3$).

Supplementary Information

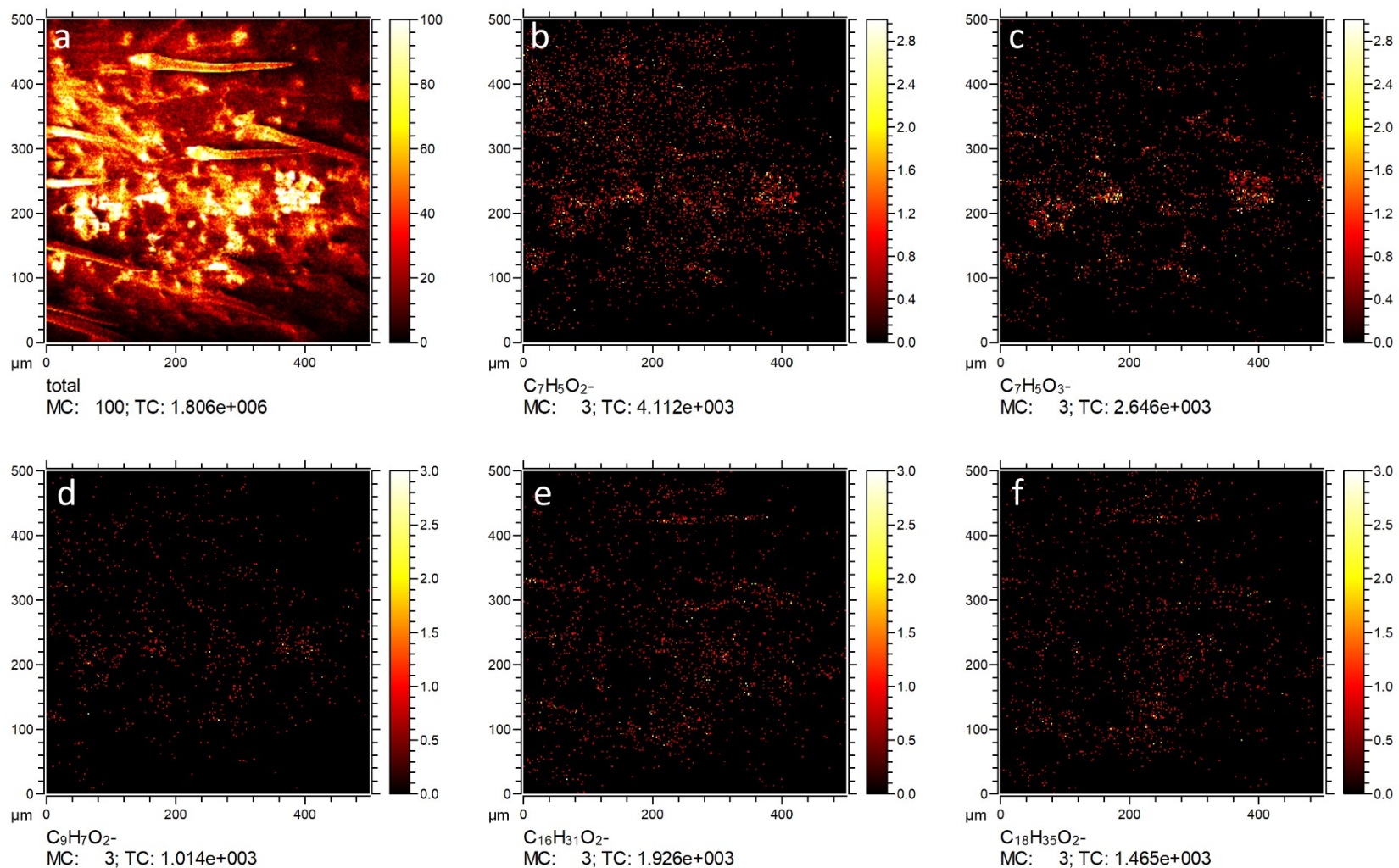


Fig. S20. Delayed extraction 2D the DI control seed of the top section in the negative mode: (a) total ions, (b) fragment of quercetin^{[1,2]B}⁻ (m/z^- 120.99, $C_7H_5O_2^-$), (c) p-hydroxybenzoic acid (m/z^- 137.02, $C_7H_5O_3^-$), (d) cinnamic acid (m/z^- 147.04, $C_9H_7O_2^-$), (e) palmitic acid (m/z^- 255.13, $C_{16}H_{31}O_2^-$), and (f) stearic acid (m/z^- 283.29, $C_{18}H_{35}O_2^-$). The scanning areas are 500 × 500 μm².

Supplementary Information

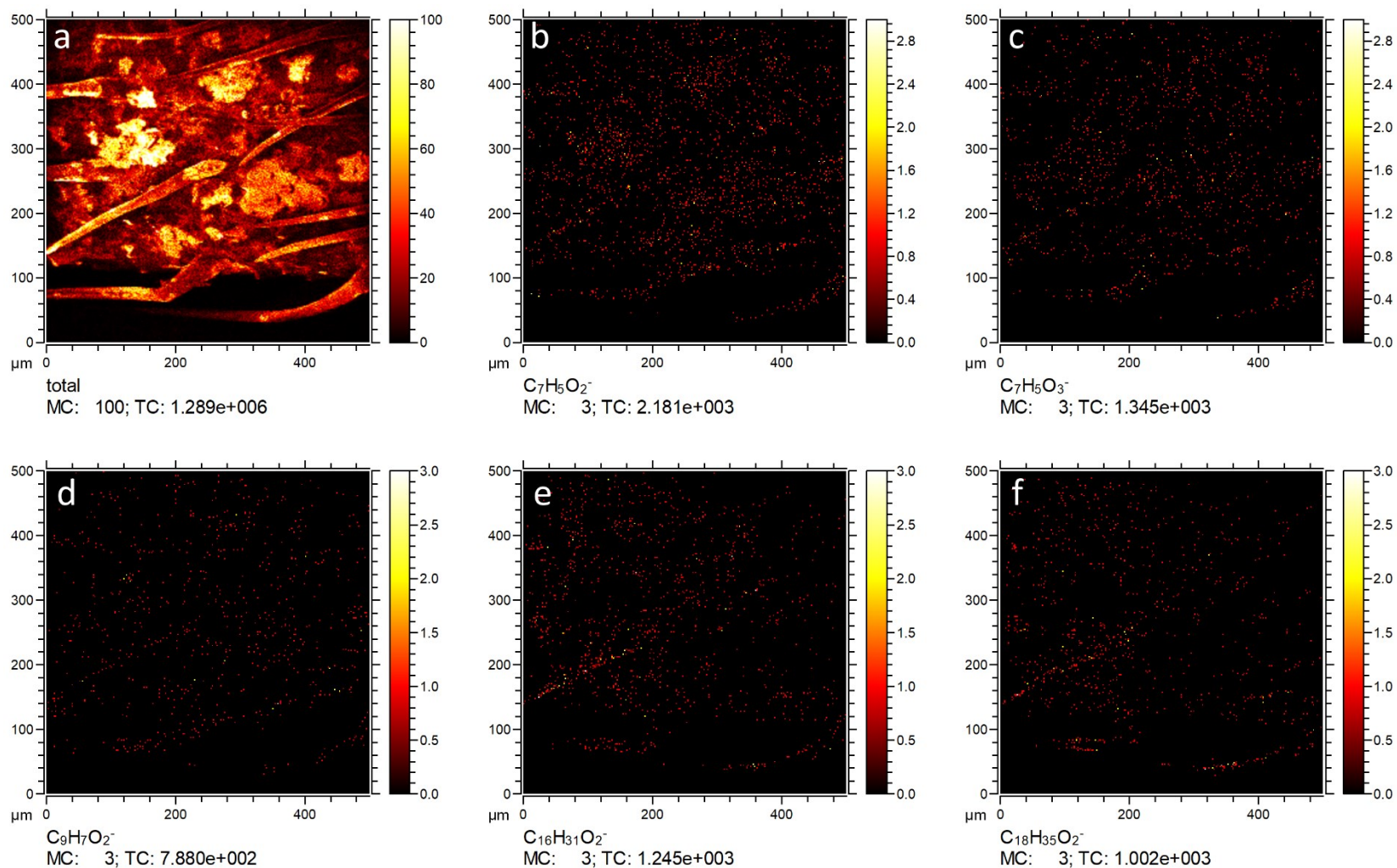


Fig. S21. Delayed extraction 2D images of the *P.*-treated seed of the top section in the negative mode: (a) total ions, (b) fragment of quercetin $[^{1,2}B]^-$ (m/z^- 120.99, $C_7H_5O_2^-$), (c) p-hydroxybenzoic acid (m/z^- 137.02, $C_7H_5O_3^-$), (d) cinnamic acid (m/z^- 147.04, $C_9H_7O_2^-$), (e) palmitic acid (m/z^- 255.13, $C_{16}H_{31}O_2^-$), and (f) stearic acid (m/z^- 283.29, $C_{18}H_{35}O_2^-$). The scanning areas are 500 × 500 μm².

Supplementary Information

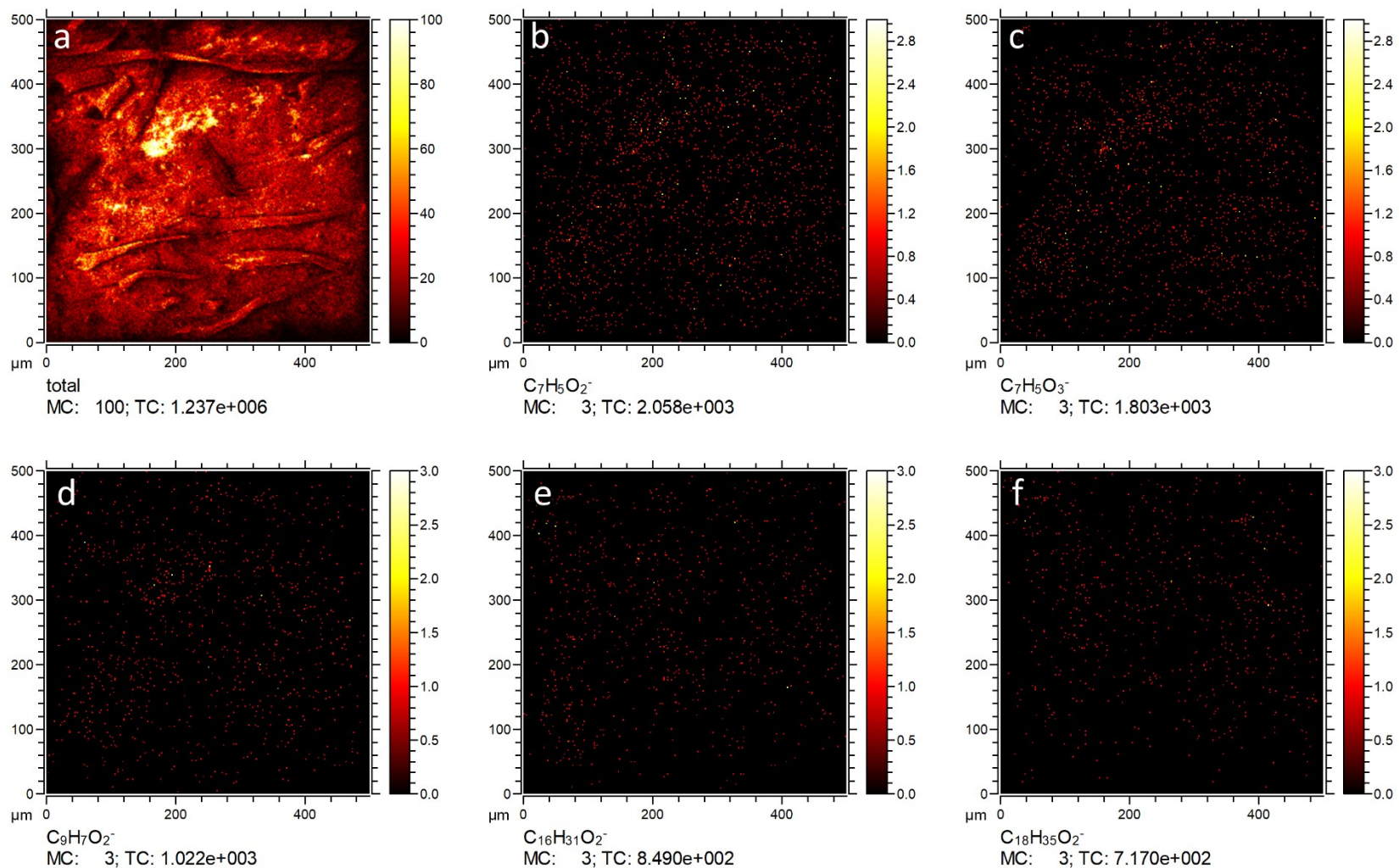


Fig. S22. Delayed extraction 2D images of the *A.*-treated seed of the top section in the negative mode: (a) total ions, (b) fragment of quercetin [^{1,2}B]⁻ (m/z^- 120.99, C₇H₅O₂⁻), (c) p-hydroxybenzoic acid (m/z^- 137.02, C₇H₅O₃⁻), (d) cinnamic acid (m/z^- 147.04, C₉H₇O₂⁻), (e) palmitic acid (m/z^- 255.13, C₁₆H₃₁O₂⁻), and (f) stearic acid (m/z^- 283.29, C₁₈H₃₅O₂⁻). The scanning areas are 500 × 500 μm².

Supplementary Information

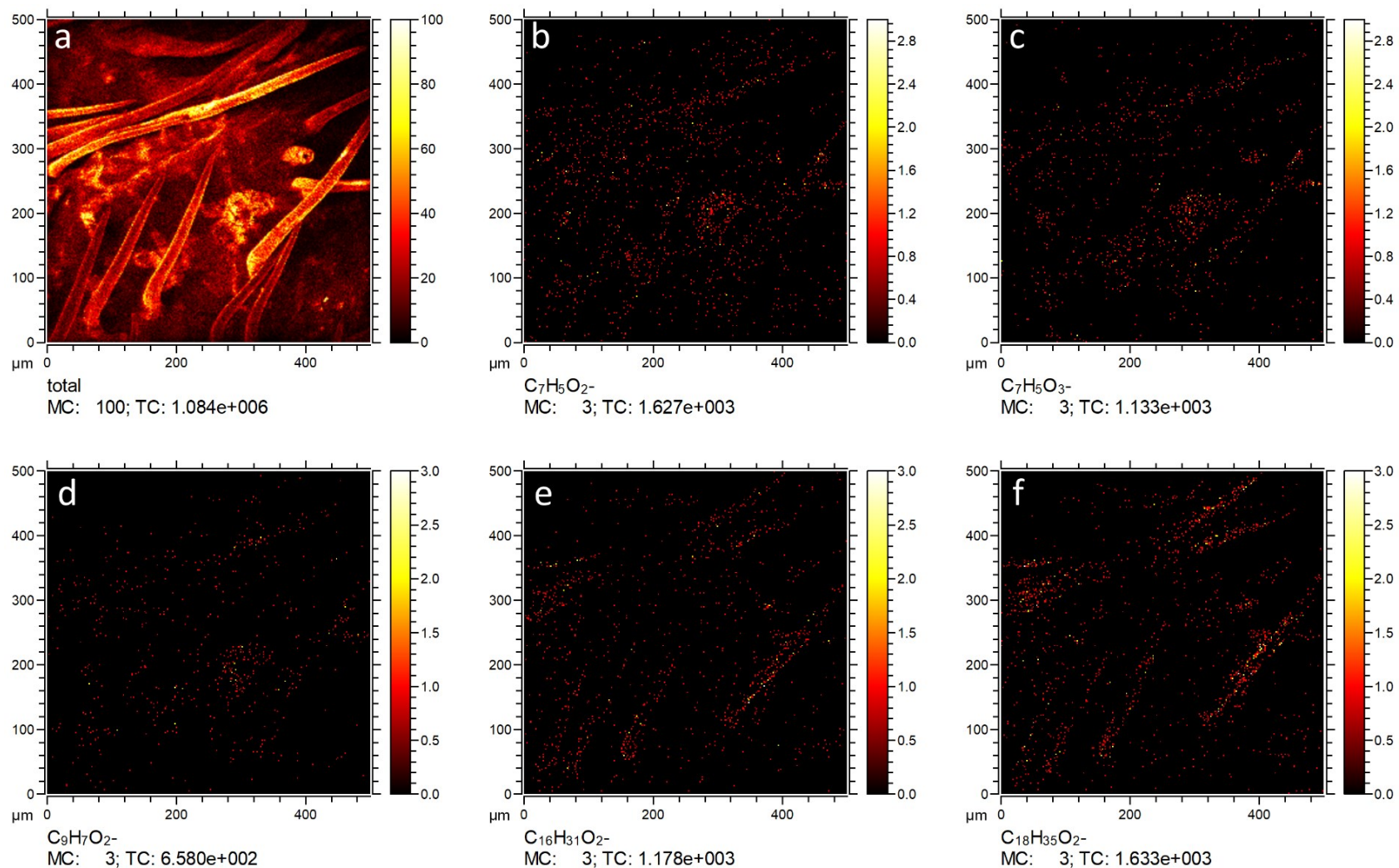


Fig. S23. Delayed extraction 2D images of the DI control seed of the bottom section in the negative mode: (a) total ions, (b) fragment of quercetin $[^{1,2}B]^-$ (m/z^- 120.99, $C_7H_5O_2^-$), (c) p-hydroxybenzoic acid (m/z^- 137.02, $C_7H_5O_3^-$), (d) cinnamic acid (m/z^- 147.04, $C_9H_7O_2^-$), (e) palmitic acid (m/z^- 255.13, $C_{16}H_{31}O_2^-$), and (f) stearic acid (m/z^- 283.29, $C_{18}H_{35}O_2^-$). The scanning areas are 500 × 500 μm².

Supplementary Information

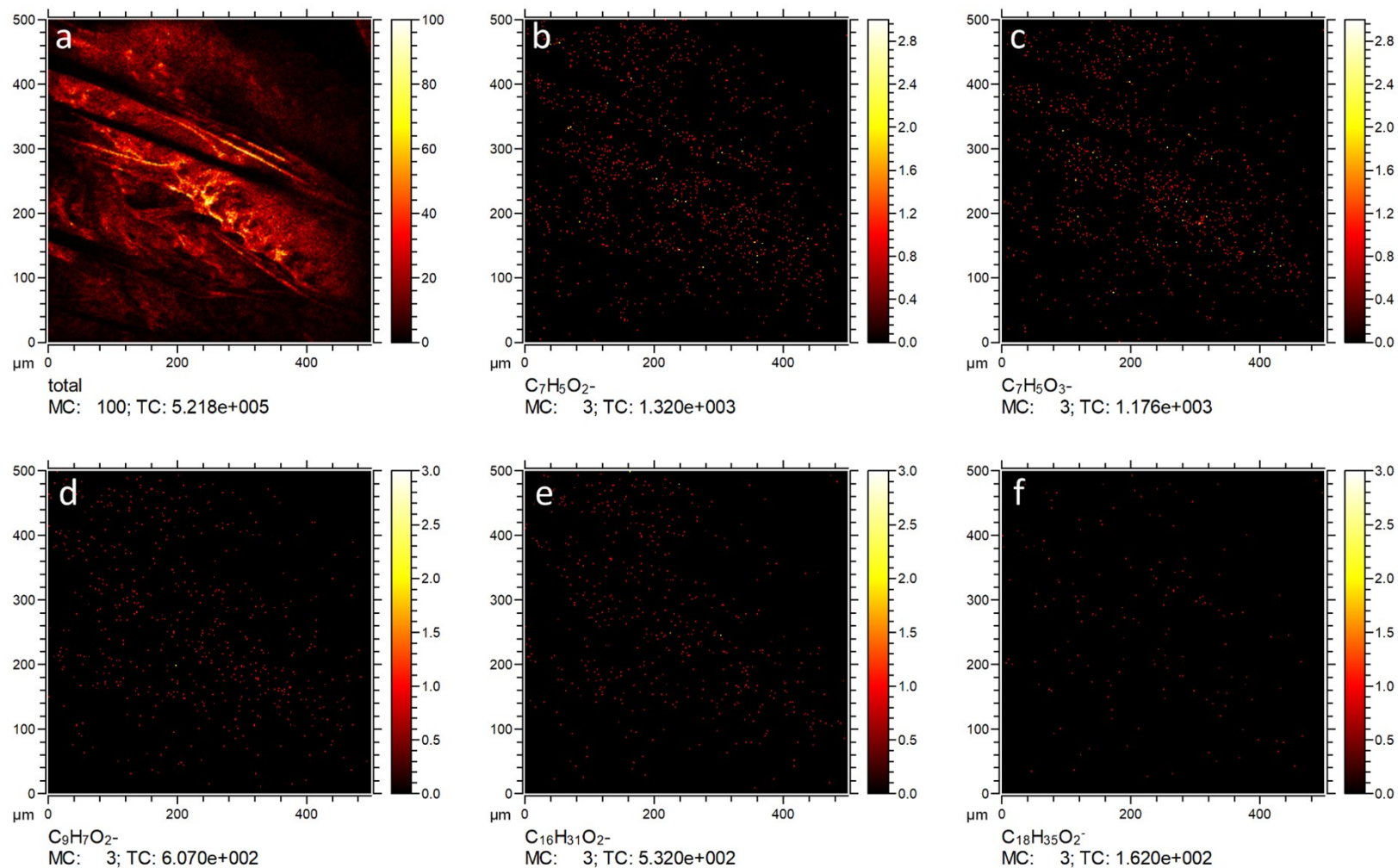


Fig. S24. Delayed extraction 2D images of the *P.*-treated seed of the bottom section in the negative mode: (a) total ions, (b) fragment of quercetin[$^{1,2}\text{B}$] $^-$ (m/z^- 120.99, $\text{C}_7\text{H}_5\text{O}_2^-$), (c) p-hydroxybenzoic acid (m/z^- 137.02, $\text{C}_7\text{H}_5\text{O}_3^-$), (d) cinnamic acid (m/z^- 147.04, $\text{C}_9\text{H}_7\text{O}_2^-$), (e) palmitic acid (m/z^- 255.13, $\text{C}_{16}\text{H}_{31}\text{O}_2^-$) and (f) stearic acid (m/z^- 283.29, $\text{C}_{18}\text{H}_{35}\text{O}_2^-$). The scanning areas are 500 \times 500 μm^2 .

Supplementary Information

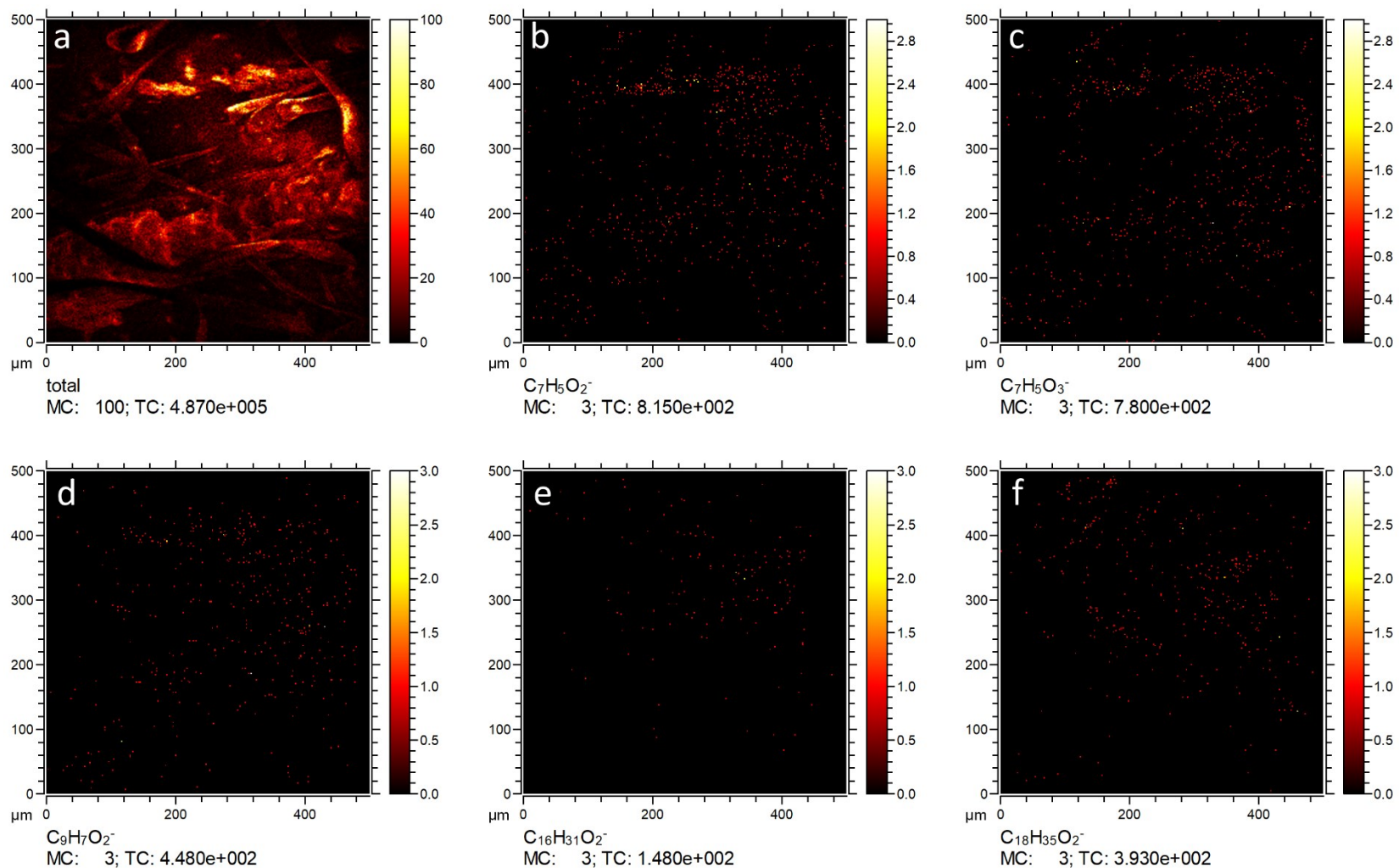


Fig. S25. Delayed extraction 2D images of the *A.*-treated seed of the bottom section in the negative mode: (a) total ions, (b) fragment of quercetin [$^{1,2}\text{B}$] $^-$ (m/z^- 120.99, $\text{C}_7\text{H}_5\text{O}_2^-$), (c) p-hydroxybenzoic acid (m/z^- 137.02, $\text{C}_7\text{H}_5\text{O}_3^-$), (d) cinnamic acid (m/z^- 147.04, $\text{C}_9\text{H}_7\text{O}_2^-$), (e) palmitic acid (m/z^- 255.13, $\text{C}_{16}\text{H}_{31}\text{O}_2^-$), and (f) stearic acid (m/z^- 283.29, $\text{C}_{18}\text{H}_{35}\text{O}_2^-$). The scanning areas are 500 × 500 μm².

Supplementary Information

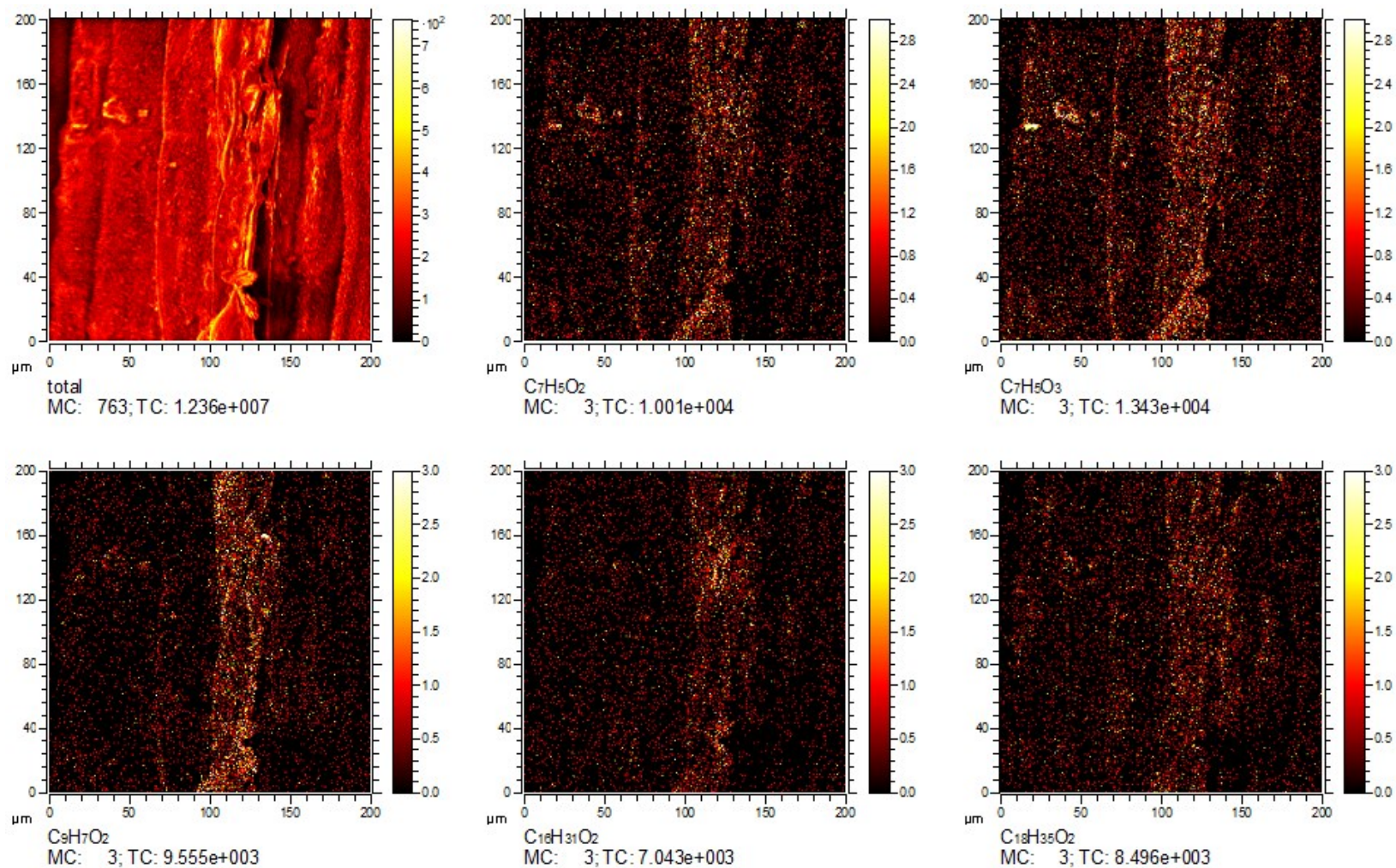


Fig. S26. High resolution 2D images of the Seteria leaf in the negative mode: (a) total ions, (b) fragment of quercetin[$^{1,2}\text{B}$] $^-$ (m/z^- 120.99, $\text{C}_7\text{H}_5\text{O}_2^-$), (c) p-hydroxybenzoic acid (m/z^- 137.02, $\text{C}_7\text{H}_5\text{O}_3^-$), (d) cinnamic acid (m/z^- 147.04, $\text{C}_9\text{H}_7\text{O}_2^-$), (e) palmitic acid (m/z^- 255.13, $\text{C}_{16}\text{H}_{31}\text{O}_2^-$), and (f) stearic acid (m/z^- 283.29, $\text{C}_{18}\text{H}_{35}\text{O}_2^-$). The scanning areas are 200 \times 200 μm^2 .

Supplementary Information

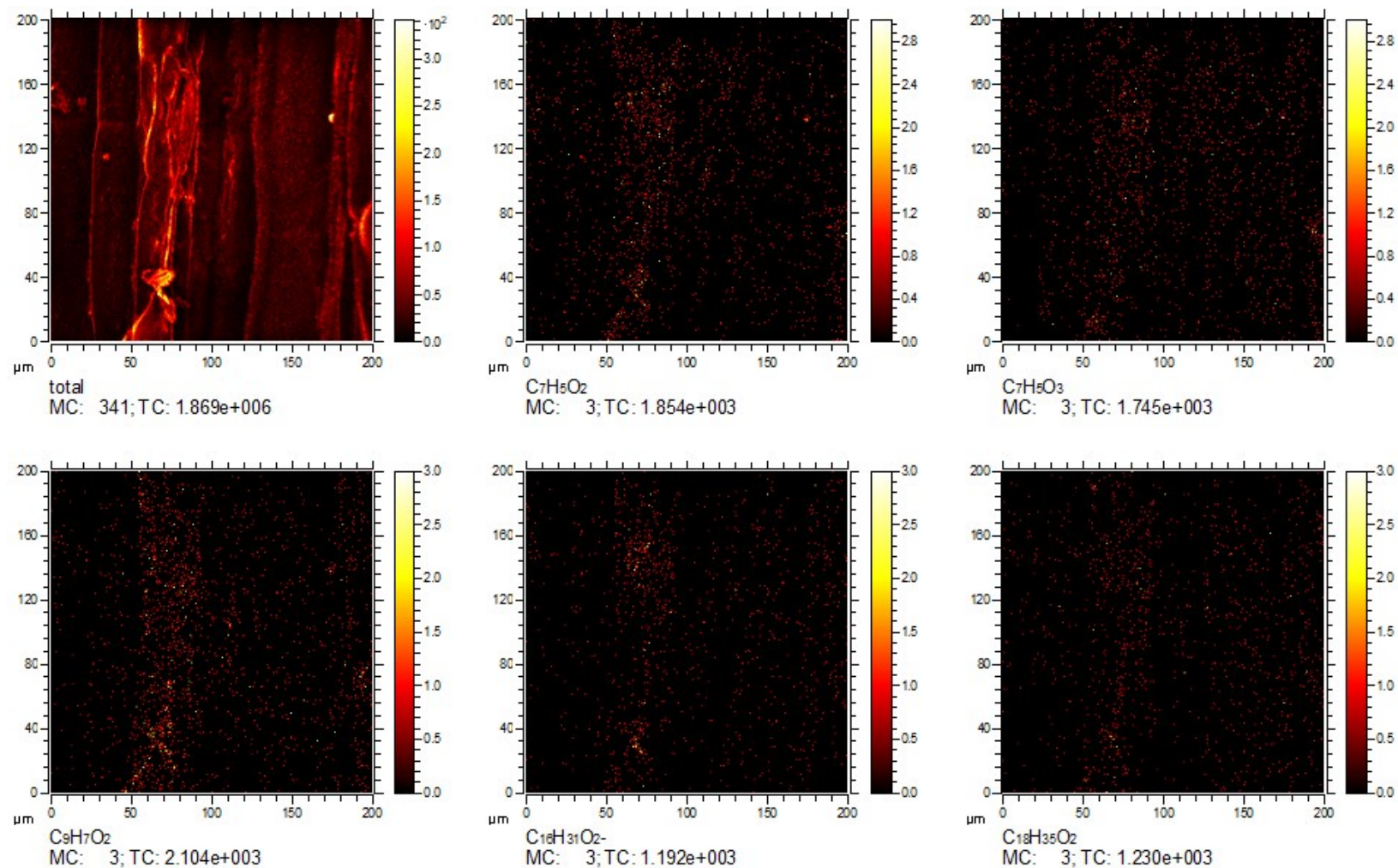


Fig. S27. Delayed extraction 2D images of the *Seteria* leaf in the negative mode: (a) total ions, (b) fragment of quercetin $[^{1,2}B]^-$ (m/z^- 120.99, $C_7H_5O_2^-$), (c) p-hydroxybenzoic acid (m/z^- 137.02, $C_7H_5O_3^-$), (d) cinnamic acid (m/z^- 147.04, $C_9H_7O_2^-$), (e) palmitic acid (m/z^- 255.13, $C_{16}H_{31}O_2^-$), and (f) stearic acid (m/z^- 283.29, $C_{18}H_{35}O_2^-$). The scanning areas are 200 × 200 μm².

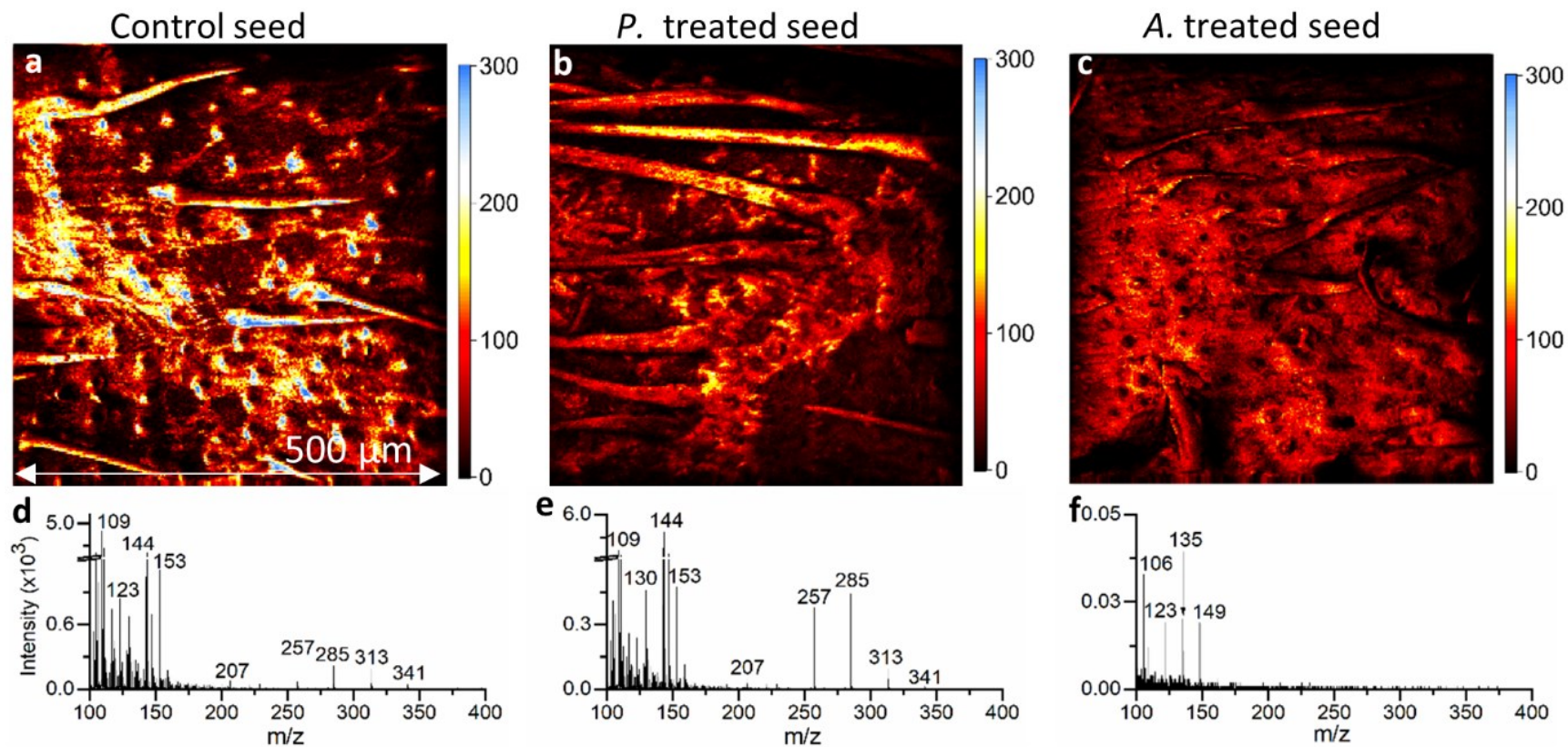


Fig. S28. Delayed extraction 2D total ion images of (a) DI control, (b) *P.*-treated, and (c) *A.*-treated *Brachypodium* seed top sections and their corresponding spectra (d-f) in m/z^+ 100 – 400 in the positive mode.

Figs. S20a-c depict the 2D total ion images in the top segment among treated seeds. Images were acquired by beam scanning an area of $500 \times 500 \mu\text{m}^2$. The blue color represents higher relative ion counts while darker color lower counts. Treated seeds show morphological differences. Figs. 20d-f show spectral results acquired from the delayed extraction mode. For example, some fatty acid peaks, such as palmitic acid (m/z^+ 257.15, $\text{C}_{16}\text{H}_{33}\text{O}_2^+$), stearic acid (m/z^+ 285.17, $\text{C}_{18}\text{H}_{37}\text{O}_2^+$), and arachidic acid (m/z^+ 313.20, $\text{C}_{20}\text{H}_{41}\text{O}_2^+$), are prominent in the DI control seed and *P.*-treated seed sections. Total intensities are weaker in the *A.*-treated seed likely due to instrument tuning before data collection.

Supplementary Information

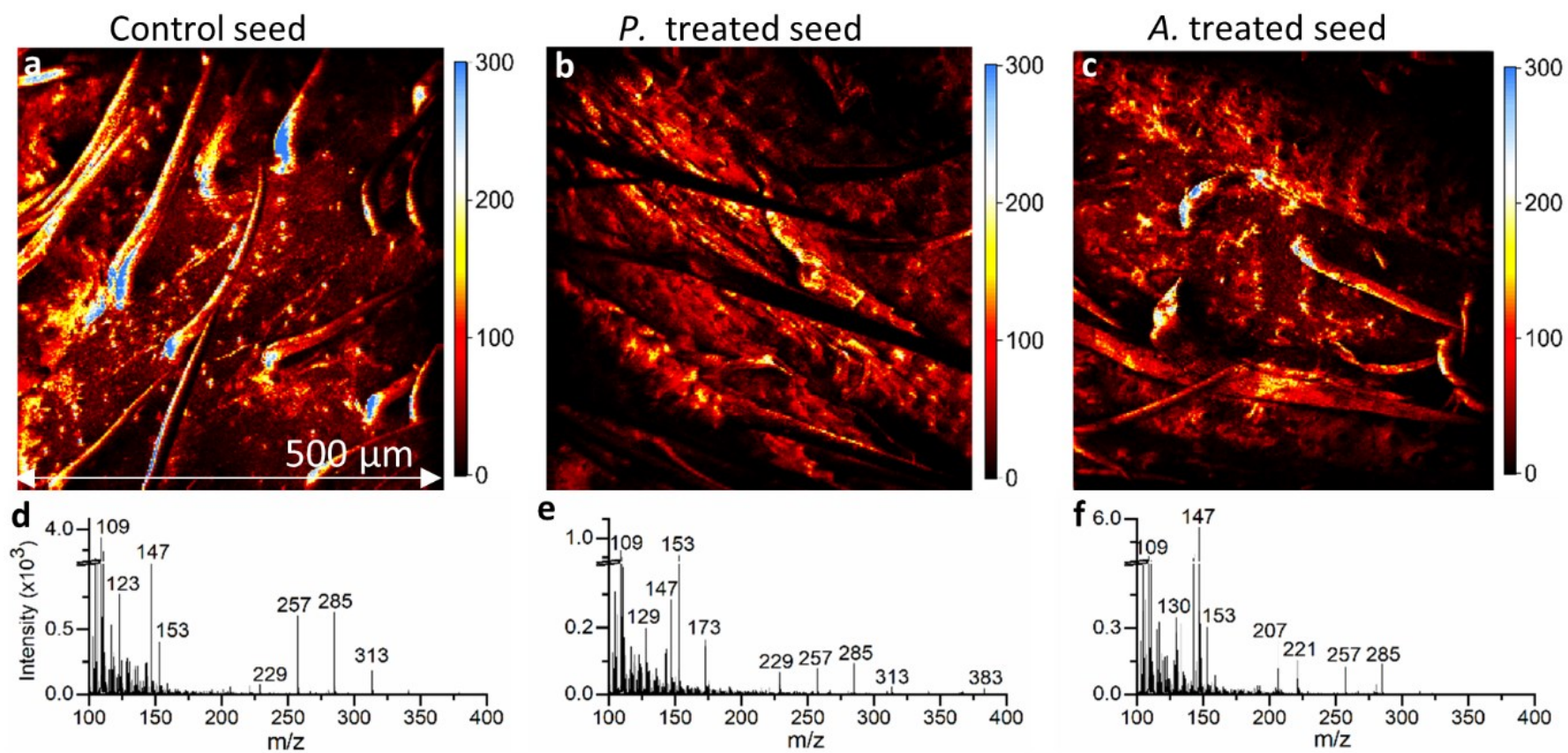


Fig. S29. Delayed extraction 2D total ion images of (a) DI control, (b) *P.*-treated, and (c) *A.*-treated *Brachypodium* seed bottom sections and their corresponding spectra (d-f) in m/z^+ 100 – 400 in the positive mode.

Figs. S21a-c depict the 2D total ion images in the bottom segment among treated seeds. Images were acquired by scanning the primary ion beam over an area of $500 \times 500 \mu\text{m}^2$. The blue color represents higher relative ion counts while darker color lower counts. PGPR-treated seeds show morphological differences. Figs. 21d-f show spectral results from the delayed extraction mode. For example, fatty acid peaks, such as palmitic acid (m/z^+ 257.15, $\text{C}_{16}\text{H}_{33}\text{O}_2^+$) and stearic acid (m/z^+ 285.17, $\text{C}_{18}\text{H}_{37}\text{O}_2^+$), are prominent in all three types of seed sections. Ions of m/z^+ 109.09 and m/z^+ 147.07 are not assigned, and they are prominent in the range of $m/z^+ \leq 200$.

Supplementary Information

Supplemental Tables

Table S1. The mass resolution of selected peaks of the delayed extraction mode.

m/z^-_{obs}	m/z^-_{the}	Formula	Mass resolution under Delayed extraction spectral mode
13.010	13.008	CH ⁻	3485
25.009	25.008	C ₂ H ⁻	1119
120.984	121.029	C ₇ H ₅ O ₂ ⁻	1880
137.019	137.024	C ₇ H ₅ O ₃ ⁻	804
147.044	147.045	C ₉ H ₇ O ₂ ⁻	1890
150.998	151.040	C ₈ H ₇ O ₃ ⁻	820
163.047	163.040	C ₆ H ₁₁ O ₅ ⁻	1177
183.049	183.045	C ₁₂ H ₇ O ₂ ⁻	1016
255.128	255.232	C ₁₆ H ₃₁ O ₂ ⁻	2141
265.277	265.217	C ₁₇ H ₂₉ O ₂ ⁻	1790
283.286	283.264	C ₁₈ H ₃₅ O ₂ ⁻	2205
311.320	311.295	C ₂₀ H ₃₉ O ₂ ⁻	2103
325.114	325.311	C ₂₁ H ₄₁ O ₂ ⁻	2175
339.357	339.326	C ₂₂ H ₄₃ O ₂ ⁻	1985
395.327	395.389	C ₂₆ H ₅₁ O ₂ ⁻	2335

m/z^-_{the} : the theoretical mass to charge ratio

m/z^-_{obs} : the observed mass to charge ratio

Supplementary Information

Table S2. Possible peak identification in the negative ion mode.

m/z^-_{obs}	m/z^-_{the}	Formula	Description	References
13.010	13.008	CH ⁻	Hydrocarbon	1
25.009	25.008	C ₂ H ⁻	Hydrocarbon	1
26.017	26.016	C ₂ H ₂ ⁻	Hydrocarbon	1
49.009	49.008	C ₄ H ⁻	Hydrocarbon	1
62.961	-	-	Not assigned	-
78.916	-	-	Not assigned	-
113.064	113.060	C ₆ H ₉ O ₂ ⁻	Fatty acids fragment	2
117.960	-	-	Not assigned	-
120.984	121.029	C ₇ H ₅ O ₂ ⁻	Fragment of quercetin ^[1,2 B-]	3
127.051	127.076	C ₇ H ₁₁ O ₂ ⁻	Fatty acids fragment	2
129.023	129.055	C ₆ H ₉ O ₃ ⁻	Tricaffeoyl-glucosyl-glucoside	4
137.019	137.024	C ₇ H ₅ O ₃ ⁻	p-Hydroxybenzoic acid	5
141.026	141.092	C ₈ H ₁₃ O ₂ ⁻	Fatty acids fragment	2
147.044	147.045	C ₉ H ₇ O ₂ ⁻	Cinnamic acid	3
150.998	151.040	C ₈ H ₇ O ₃ ⁻	Vanillin	3
153.018	153.019	C ₇ H ₅ O ₄ ⁻	Protocatechuic acid	3
163.047	163.040	C ₆ H ₁₁ O ₅ ⁻	p-Coumaric acid	3
169.017	169.014	C ₇ H ₅ O ₅ ⁻	Gallic acid	6
180.042	180.063	C ₆ H ₁₂ O ₆ ⁻	Glucose	7
183.049	183.045	C ₁₂ H ₇ O ₂ ⁻	Fragment of galangin	3
222.975	223.170	C ₁₄ H ₂₃ O ₂ ⁻	Myristic acid	8
225.128	225.185	C ₁₄ H ₂₅ O ₂ ⁻	Myristic acid	8
227.081	227.201	C ₁₄ H ₂₇ O ₂ ⁻	Myristic acid	8
237.244	237.222	C ₁₆ H ₂₉ O ⁻	Palmitic acid	9
241.057	-	-	Not assigned	-
252.962	253.050	C ₁₅ H ₉ O ₄ ⁻	Dihydroxyflavone	3
255.128	255.232	C ₁₆ H ₃₁ O ₂ ⁻	Palmitic acid	8
265.277	265.217	C ₁₇ H ₂₉ O ₂ ⁻	Margaric acid	8
281.282	281.248	C ₁₈ H ₃₃ O ₂ ⁻	Oleic acid	10
283.286	283.264	C ₁₈ H ₃₅ O ₂ ⁻	Stearic acid	8
293.303	293.248	C ₁₉ H ₃₃ O ₂ ⁻	Nonadecylic acid	7
311.320	311.295	C ₂₀ H ₃₉ O ₂ ⁻	Arachidic acid	8
325.114	325.311	C ₂₁ H ₄₁ O ₂ ⁻	Heneicosanoic acid	7
339.357	339.326	C ₂₂ H ₄₃ O ₂ ⁻	Docosanoic acid	11
353.939	-	-	Not assigned	-
379.107	-	-	Not assigned	-
395.327	395.389	C ₂₆ H ₅₁ O ₂ ⁻	Cerotic acid	12

m/z^-_{obs} : the observed mass to charge ratio

m/z^-_{the} : the theoretical mass to charge ratio

Supplementary Information

Table S3. Possible peak identification in the positive ion mode.

m/z^+_{obs}	m/z^+_{the}	Formula	Chemical description	References
22.991	22.990	Na ⁺	Inorganic ion	1
27.024	27.023	C ₂ H ₃ ⁺	Hydrocarbon	1
29.040	29.039	C ₂ H ₅ ⁺	Hydrocarbon	1
38.966	38.964	K ⁺	Inorganic ion	1
41.039	41.039	C ₃ H ₅ ⁺	Hydrocarbon	1
43.056	43.055	C ₃ H ₇ ⁺	Hydrocarbon	1
55.056	55.055	C ₄ H ₇ ⁺	Hydrocarbon	1
57.070	57.070	C ₄ H ₉ ⁺	Hydrocarbon	1
67.056	67.055	C ₅ H ₇ ⁺	Hydrocarbon	1
69.071	69.070	C ₅ H ₉ ⁺	Hydrocarbon	1
71.092	71.086	C ₅ H ₁₁ ⁺	Hydrocarbon	1
81.070	81.070	C ₆ H ₉ ⁺	Hydrocarbon	1
105.074	105.070	C ₈ H ₉ ⁺	Hydrocarbon	1
109.097	109.102	C ₈ H ₁₃ ⁺	Hydrocarbon	7
130.020	-	-	Not assigned	-
144.031	-	-	Not assigned	-
147.007	-	-	Not assigned	-
158.851	159.066/159.029	C ₇ H ₁₁ O ₄ ⁺ /C ₆ H ₇ O ₅ ⁺	Polymer/Protein	9
165.071	165.059	C ₁₀ H ₁₃ O ₂ ⁺	α -tocopherol fragment	13
174.957	175.063	C ₁₀ H ₉ NO ₂ ⁺	Indole-3-acetic acid	14
206.974	-	-	Not assigned	-
221.069	-	-	Not assigned	-
229.230	229.217	C ₁₄ H ₂₉ O ₂ ⁺	Myristic acid	8
257.151	257.248	C ₁₆ H ₃₃ O ₂ ⁺	Palmitic acid	8
285.170	285.279	C ₁₈ H ₃₇ O ₂ ⁺	Stearic acid	8
313.205	313.311	C ₂₀ H ₄₁ O ₂ ⁺	Arachidic acid	12
341.368	341.342	C ₂₂ H ₄₃ O ₂ ⁺	Docosanoic acid	11
364.477	-	-	Not assigned	-
383.105	-	-	Not assigned	-

m/z^+_{obs} : the observed mass to charge ratio

m/z^+_{the} : the theoretical mass to charge ratio

Supplementary Information

Table S4. Representative fatty acid reference spectral information in the negative and positive ion mode.

Reference	Negative mode			Positive mode		
	Formula	m/z_{obs}^-	m/z_{the}^-	Formula	m/z_{obs}^+	m/z_{the}^+
Myristic acid	$\text{C}_{14}\text{H}_{27}\text{O}_2^-$	227.163	227.201	$\text{C}_{14}\text{H}_{29}\text{O}_2^+$	229.192	229.217
Margaric acid	$\text{C}_{17}\text{H}_{29}\text{O}_2^-$	265.230	265.217			
Stearic acid	$\text{C}_{18}\text{H}_{35}\text{O}_2^-$	283.295	283.264	$\text{C}_{18}\text{H}_{37}\text{O}_2^+$	285.210	285.279
Arachidic acid	$\text{C}_{20}\text{H}_{39}\text{O}_2^-$	311.302	311.295	$\text{C}_{20}\text{H}_{41}\text{O}_2^+$	313.277	313.311
Heneicosanoic acid	$\text{C}_{21}\text{H}_{41}\text{O}_2^-$	325.279	325.311			
Docosanoic acid	$\text{C}_{22}\text{H}_{43}\text{O}_2^-$	339.345	339.326	$\text{C}_{22}\text{H}_{43}\text{O}_2^+$	341.320	341.342
Cerotic acid	$\text{C}_{26}\text{H}_{51}\text{O}_2^-$	395.401	395.389			

m/z_{obs} : the observed mass to charge ratio

m/z_{the} : the theoretical mass to charge ratio

Supplementary Information

References

1. W. Li, H. Li, J. Li, X. Cheng, Z. Zhang, F. Chai, H. Zhang, T. Yang, P. Duan, D. Lu and Y. Chen, *J. Environ. Sci.*, 2018, **69**, 61-76.
2. K. Keune and J. J. Boon, *Surf. Interface Anal.*, 2004, **36**, 1620-1628.
3. P. Ristivojević, I. Dimkić, E. Guzelmeric, J. Trifković, M. Knežević, T. Berić, E. Yesilada, D. Milojković-Opsenica and S. Stanković, *LWT-Food Sci. Technol.*, 2018, **95**, 367-379.
4. Z. Benayad, C. Gomez-Cordoves and N. E. Es-Safi, *Int. J. Mol. Sci.*, 2014, **15**, 20668-20685.
5. A. Seyer, J. Einhorn, A. Brunelle and O. Laprevote, *Anal. Chem.*, 2010, **82**, 2326-2333.
6. L. S. Chua, N. A. Latiff, S. Y. Lee, C. T. Lee, M. R. Sarmidi and R. A. Aziz, *Food Chem.*, 2011, **127**, 1186-1192.
7. NIH, PubChem, <http://pubchem.ncbi.nlm.nih.gov>, (accessed March 16, 2020, 2020).
8. T. Leefmann, C. Heim, A. Kryvenda, S. Siljeström, P. Sjövall and V. Thiel, *Org. Geochem.*, 2013, **57**, 23-33.
9. Y. Ding, Y. Zhou, J. Yao, C. Szymanski, J. Fredrickson, L. Shi, B. Cao, Z. Zhu and X. Y. Yu, *Anal. Chem.*, 2016, **88**, 11244-11252.
10. S. Liu, W. Ruan, J. Li, H. Xu, J. Wang, Y. Gao and J. Wang, *Mycopathologia*, 2008, **166**, 93-102.
11. Y. Li, Y. H. Li, P. Yang, H. A. Zhang and D. He, *Hortic. Environ. Biotechnol.*, 2017, **58**, 334-341.
12. A. A. Millar, M. A. Smith and L. Kunst, *Trends Plant Sci.*, 2000, **5**, 95-101.
13. E. B. Monroe, J. C. Jurchen, J. Lee, S. S. Rubakhin and J. V. Sweedler, *J. Am. Chem. Soc.*, 2005, **127**, 12152-12153.
14. M. S. Greenwood, S. Shaw, J. R. Hillman, A. Ritchie and M. B. Wilkins, *Planta*, 1972, **108**, 179-183.